Equilibrium Star Formation In A Constant Q Disk: Model Optimisation and Initial Tests

Zheng Zheng[1], Gerhardt R. Meurer[2], Timothy M. Heckman[1], David Thilker [1],
and Martin Zwaan[3]

ABSTRACT

We develop a model for the distribution of the ISM and star formation in galaxies based on recent studies that indicate that galactic disks stabilise to a constant stability parameter, which we combine with prescriptions of how the phases of the ISM are determined and for the Star Formation Law (SFL). The model predicts the gas surface mass density and star formation intensity of a galaxy given its rotation curve, stellar surface mass density and the gas velocity dispersion. This model is tested on radial profiles of neutral and molecular ISM surface mass density and star formation intensity of 12 galaxies selected from the THINGS sample. Our tests focus on intermediate radii (0.3 to 1 times the optical radius) because there are insufficient data to test the outer disks and the fits are less accurate in detail in the centre. Nevertheless, the model produces reasonable agreement with ISM mass and star formation rate integrated over the central region in all but one case. To optimise the model, we evaluate four recipes for the stability parameter, three recipes for apportioning the ISM into molecular and neutral components, and eight versions of the SFL. We find no clear-cut best prescription for the two-fluid (gas and stars) stability parameter Q_{2f} and therefore for simplicity, we use the Wang & Silk (1994) approximation (Q_{WS}). We found that an empirical scaling between the molecular to neutral ISM ratio (R_{mol}) and the stellar surface mass density proposed by Leroy et al. (2008) works marginally better than the other two prescriptions for this ratio in predicting the ISM profiles, and noticeably better in predicting star formation intensity from the ISM profiles produced by our model with the SFLs we tested. Thus in the context of our modeled ISM profiles, the linear molecular SFL and the two-component SFL (Krumholz et al. 2009b) work better than the other prescriptions we tested. We incorporate these relations into our 'Constant Q disk' (CQ-disk) model.

Keywords: galaxies: ISM - kinematics and dynamics - star formation

[1]Department of Physics and Astronomy, Johns Hopkins University, 3701 San Martin Drive, Baltimore, MD 21218, USA

[2]International Centre for Radio Astronomy Research, The University of Western Australia, M468, 35 StirlingHighway, Crawley, WA 6009, Australia

[3]European Southern Observatory, Karl-Schwarzschild-Str. 2, 85748 Garching, Germany

1.   Introduction

The processes in the interstellar medium (ISM, or gas) that determine its distribution, structure, and the formation of stars are multiple, very complex, and operate on atomic to galactic size scales (see e.g. McKee & Ostriker 2007). This makes it difficult to develop a comprehensive model for the distribution of gas and star formation in galaxies from first principles. Fortunately, normal galaxies are usually in a marginally stable equilibrium state. Here we use this fact as the basis of a model for the distribution of gas in galaxies, and with some additional assumptions we extend this into a model of the star formation distribution. Our aim is to construct an easy to implement model for the distribution of gas and star formation in galaxies that can be used to compare to observations and to easily create realistic simulated galaxies. Our approach also allows difficult to observe properties of galaxies (e.g. the molecular ISM distribution) to be inferred from those that are relatively easy to determine or infer (the stellar mass profile and rotation curve).

Star formation has long been believed to be related to disk (in)stability. Major studies (e.g. Toomre 1964; Wang & Silk 1994; Rafikov 2001; Romeo & Wiegert 2011; Elmegreen 2011) have been carried out on gravitational disk stability since the 1960s and the theory of this subject is well developed. However, as early as 1972, Quirk claimed that the whole galactic disk should be marginally stable due to negative feedback mechanism. He used this assumption to predict the gas surface density profile; his model roughly matches the observations in the outer regions of his sample galaxies but overestimates the densities in the inner half of the galaxies. Since then, observational evidence for Quirk's statement that disk galaxies are usually in a marginally stable state has mounted and been noticed in various studies (e.g. Kennicutt 1989; van der Hulst et al. 1993; Leroy et al. 2008).

The gravitational stability parameter Q (see section 2.1 for details) for a single component thin disk was first derived by Toomre (1964). Kennicutt (1989) used a sample of tens of galaxies to show that there is very little star formation where Q is above some critical threshold. Martin & Kennicutt (2001) confirmed the result using more recent data. However a single fluid Q does not accurately indicate the stability of a real disk which contains both stars and gas. Jog & Solomon (1984) derived the two-fluid (stars and gas) stability parameter Q_{2f} for a thin disk. Rafikov (2001) improved the derivation by considering the stellar component as collisionless, yielding a rigorous but elaborate form of the stability parameter, Q_R. Wang & Silk (1994) proposed an approximation for the two-fluid stability parameter, Q_{WS}, which is widely used because of its simple form. More recently, Romeo & Wiegert (2011) reexamined the Wang & Silk (1994) approximation and gave a simple but more accurate effective two-fluid stability parameters for both an infinitesimally thin ($Q_{RW,thin}$) and finite thickness ($Q_{RW,thick}$) galactic disks.

Inspired by the Quirk (1972) and recent studies on disk stability theory and star formation laws, we develop and test the 'Constant Q disk' (CQ-disk) model, which we define as: A two-fluid (gas+stars) axisymmetric thin disk will evolve into a marginally stable state with a constant stability parameter Q_{2f} through out the galactic disk. The basic idea for this model is to use the constancy of the two-fluid stability parameter to predict the distribution of gas and then use empirical molecular-to-neutral gas ratio (R_{mol}) relations and the best star formation law (SFL) to predict the distribution of neutral and molecular gas as well as star formation rate. Here we compare the observed distribution of the ISM, and star formation in a small sample of galaxies to our model in order to test our assumptions and to optimise the model by trialling different recipes for its key ingredients (Q_{2f}, R_{mol}, and the SFL).

The outline of our paper is as follows: section 2 briefly introduces background information, e.g. the gravitational stability parameter, molecular-to-neutral gas ratio model, and star formation laws; section 3 presents the detailed model we construct; section 4 gives a brief description of our sample galaxies; section 5 shows the results; in section 6 we discuss the assumption and implications of our model; and in section 7 we discuss further tests and possible uses of our model.

Through out this paper, we are only concerned with the large scale star formation in the galactic disk, hence we suppose the disk is axisymmetric and focus on the radial profiles of various physical quantities. As our research progressed it became useful to divide the galactic disk in to three regions: central (within $0.3r_{25}$), intermediate ($0.3 \sim 1r_{25}$) and outer ($> r_{25}$), where r_{25} is the optical radius, defined by where the B band surface brightness reaches 25 mag arcsec^{-2}. In general, our model works best in the intermediate radii, and much of the testing of the model is limited to these radii. The profiles we create often do not match the observations in detail in the central region, although, as we will show, the match to quantities integrated over the central region is reasonable. We can not test our star formation models in the outer disk because the star formation intensity was not measured beyond r_{25} in our data sources. In Meurer et al. (2013) we discuss the expected ISM structure in the outer disk. There we showed that a gas dominated constant Q outer disk should have a surface mass density fall-off with the same profile as the dark matter for systems with a flat rotation curve, thus explaining the close relationship between dark matter and HI (Bosma 1981; Hoekstra et al. 2001; Hessman & Ziebart 2011). The other reason that we make these divisions is that the RCs are generally more reliable in the intermediate disk: there are less or even no data points in the central regions, while often warps and asymmetries are present in the outer regions.

2. Background information

2.1. Brief introduction to the gravitational stability parameter

Toomre (1964) showed that galactic disks can be unstable to axis-symmetric perturbations, and that the stability of a thin disk to such a perturbation can be represented quantitatively in a single parameter Q. Following Toomre (1964), Wang & Silk (1994), and Rafikov (2001), we express the stability parameter for a gaseous disk:

$$Q_g = \frac{\sigma_g \kappa}{\pi G \Sigma_g}, \tag{1}$$

where σ_g is the gas velocity dispersion. Typically σ_g is assumed to be constant (e.g. Leroy et al. 2008, hereafter L08), although observations show that it typically slowly varies with radius (e.g. Tamburro et al. 2009; O'Brien et al. 2010). G is the gravitational constant, Σ_g is the gas surface mass density and κ is the epicyclic frequency which can be calculated from the rotation curve using

$$\kappa = \frac{v}{r} \sqrt{2 \left(1 + \frac{r}{v} \frac{dv}{dr} \right)}, \tag{2}$$

where v is the circular velocity of the gas at a distance r from the galactic centre. Toomre's Q parameter can be an indicator for widespread star formation: a large stability parameter ($Q_g > 1$) means that pressure and centrifugal forces are sufficient to support the disk and thus it is stable, while a small $Q_g(< 1)$ means the gravity exceeds the internal support and the disk will collapse, resulting in widespread star formation (Kennicutt 1989; van der Hulst et al. 1993; Martin & Kennicutt 2001).

For a single component stellar disk, we can use a similar parameter, Q_s, to indicate gravitational stability of the stars [1] :

$$Q_s = \frac{\sigma_{s,r} \kappa}{\pi G \Sigma_s}, \tag{3}$$

where Σ_s is the star surface mass density and $\sigma_{s,r}$ is the radial component of the stellar velocity dispersion (Jog & Solomon 1984; Wang & Silk 1994; Rafikov 2001). We follow the estimation of $\sigma_{s,r}$ given by L08: assuming a typical fixed shape to the velocity dispersion ellipsoid, we have

$$\sigma_{s,r} = 1.67 \sigma_{s,z}, \tag{4}$$

---

[1]This is originally defined as $Q_s = \sigma_{s,r}\kappa/3.36G\Sigma_s$ (Toomre 1964; Binney & Tremaine 2008), but redefined as the equation shown above by later authors e.g. Wang & Silk (1994); Rafikov (2001) in order to use a more consistent expression with regards to Q_g.

where $\sigma_{s,z}$ is the z-direction component of the stellar velocity dispersion and using the standard relationship between this, disk scale height h_s, and mass density for an isothermal disk (e.g. van der Kruit 1988), we have

$$\sigma_{s,z} = \sqrt{2\pi G \Sigma_s h_s}. \tag{5}$$

Here h_s is assumed to be a constant through out the galaxy disk (e.g. as done by L08). Since, h_s is difficult to measure unless the galaxy is viewed edge-on, we follow L08 and use the exponential stellar disk's scale length, l_s, to estimate it. Using the average flattening ratio $l_s/h_s = 7.3 \pm 2.2$, measured by Kregel et al. (2002), we then obtain

$$\sigma_{s,r} \approx 1.55\sqrt{G\Sigma_s l_s}. \tag{6}$$

Galactic disks are composed of both gas and stars. Thus, we need to consider both of them in a more sophisticated disk stability theory. There have been numerous studies on the two-fluid disk stability theory and therefore different forms of two-fluid stability parameters, Q_{2f}. Here we introduce four of them:

Jog & Solomon (1984) explored the gravitational stability of a two-fluid thin disk. Later-on, Rafikov (2001) extended this work by treating the stellar part of the disk as collisionless and gave an explicit expression for the total stability parameter $Q_{\rm R}$:

$$\frac{1}{Q_R} = \frac{1}{Q_s}\frac{2}{1/q + q} + \frac{1}{Q_g}\frac{2}{yq + 1/yq}, \tag{7}$$

where

$$y = \sigma_g/\sigma_{s,r}, \tag{8}$$

and $q = k\sigma_{s,r}/\kappa$, with k the wave number of the instability being considered. We take k to be the wavenumber of the most unstable mode in our calculations (L08). In this paper, we make a coarse searching through the parameter space of k and find the value which gives the lowest gas surface mass density. We find that the galaxies studied here have $\lambda = 2\pi/k = 2 - 5 kpc$, consistent with the result of L08.

Although the Rafikov (2001) derivation of the two-fluid stability parameter is quite rigorous, it is complicated and wavenumber dependent, making it hard to use. Wang & Silk (1994) give a much simpler form, $Q_{\rm WS}$:

$$\frac{1}{Q_{\rm WS}} = \frac{1}{Q_g} + \frac{1}{Q_s}. \tag{9}$$

It is widely used by astronomers (e.g. Martin & Kennicutt 2001) although the analysis deriving it has been criticised (Jog 1996). Romeo & Wiegert (2011) improved the Wang & Silk

(1994) approximation and proposed an effective Q parameter for a two-fluid infinitesimally thin disk, $Q_{\mathrm{RW,thin}}$:

$$\frac{1}{Q_{\mathrm{RW,thin}}} = \begin{cases} \dfrac{W}{Q_s} + \dfrac{1}{Q_g} & \text{if } Q_s \geq Q_g \,, \\[1.5em] \dfrac{1}{Q_s} + \dfrac{W}{Q_g} & \text{if } Q_g \geq Q_s \,; \end{cases} \tag{10}$$

where

$$W(y) = \frac{2}{y + 1/y}, \tag{11}$$

and y is defined above in Eq. 8.

In reality, disks are not infinitesimally thin, and the thickness of the disk has a stabilising effect. Therefore, Romeo & Wiegert (2011) also give an expression for a disk of finite thickness, $Q_{\mathrm{RW,thick}}$:

$$\frac{1}{Q_{\mathrm{RW,thick}}} = \begin{cases} \dfrac{W}{T_s Q_s} + \dfrac{1}{T_g Q_g} & \text{if } T_s Q_s \geq T_g Q_g \,, \\[1.5em] \dfrac{1}{T_s Q_s} + \dfrac{W}{T_g Q_g} & \text{if } T_g Q_g \geq T_s Q_s \,; \end{cases} \tag{12}$$

where T is a factor, by which the stability parameter of each component increases, reflecting the effect of the thickness of the disk. The factor T depends on the ratio of vertical to radial velocity dispersion: $T = 0.8 + 0.7(\sigma_z/\sigma_r)$. So that we have $T_g \approx 1.5$ for gas, and $T_s \approx 1.22$ for stars.

Kennicutt (1989) showed that Q_g values for 15 disk galaxies are almost a constant. Similarly Meurer et al. (2013) used more recent measurements to show that Q_g is constant over a large fraction of the outer disks of galaxies where HI dominates the mass. Boissier et al. (2003); Martin & Kennicutt (2001) tested the Wang & Silk (1994) Q_{WS} on more disk galaxies and got a similar result. L08 used the Rafikov (2001) Q_{R} in testing the star formation threshold for 23 nearby galaxies and get a remarkably flat Q_{R} thorough the optically bright part of galactic disks with $Q_{\mathrm{R}} \sim 1.3 - 2.5$.

One plausible explanation for this phenomena is self-regulation by star formation (Burton et al. 1992; Elmegreen 2011): an unstable disk (low Q) will collapse and commence widespread star formation. The star formation will consume most of the gas in a short time (Quirk 1972), also the resulting winds from high mass stars and supernovae explosions will expel part of the gas out of the galactic disk (Dutton 2009; Heckman et al. 1990) and heat up the remaining gas (Tamburro et al. 2009). This will increase Q by lowering Σ_g and increasing σ_g and thus make the disk more stable. On the other hand, a stable disk (high Q) will have

suppressed star formation because the gas can not collapse. This means less heating of the ISM through winds and supernovae, and hence a relative cooling and lowering of σ_g, thus decreasing Q.

Thus a negative feedback system is set up and it will finally come to a stable equilibrium state. Here we suppose that galaxies equilibrate to the same Q at all radii through this local feedback cycle: regions of low Q heat up locally due to feedback, while regions of high Q cool due to relative lack of star formation. We test whether Q is constant within the optically bright portion of galaxies, and consider whether Q may be constant within a galaxy, but vary from galaxy to galaxy. This might happen if the balance in the local support between epicyclic frequency κ and velocity dispersion σ varies due to changes in the relative importance of angular momentum and feedback, perhaps due to initial mass function variations (Meurer et al. 2009) or metallicity dependent cooling.

2.2. Brief introduction to R_{mol} relations

It is useful to have an accurate prescription for determining the molecular to neutral ratio ($R_{\mathrm{mol}} \equiv \Sigma_{\mathrm{H_2}}/\Sigma_{\mathrm{HI}}$) because these phases of the ISM are measured with separate observations and because it is generally believed that star formation is more related to the the molecular rather than the atomic gas. In practice the molecular data has been more expensive to obtain than HI data and requires use of tracers of H_2 like CO emission. The advent of new facilities like SMA, CARMA and ALMA may change these economics.

Various simple prescriptions for determining R_{mol} have been raised in previous studies (cf. L08 and references therein). L08 used high quality HI and CO data to assess four of the most popular R_{mol} prescriptions and found two that worked well. The first is purely empirical and involves just the stellar surface mass density (we call this the SR relation or $R_{\mathrm{mol,s}}$)

$$R_{\mathrm{mol,s}} = \frac{\Sigma_s}{81\,M_\odot\,pc^{-2}}. \tag{13}$$

The other uses hydrostatic pressure P_h as a parameter (the PR relation or $R_{\mathrm{mol,p}}$) and is

$$R_{\mathrm{mol,p}} = \left(\frac{P_h}{1.7 \times 10^4\,cm^{-3}\,K\,k_B}\right)^{0.8}, \tag{14}$$

where P_h is given by Elmegreen (1989) as

$$P_h = \frac{\pi}{2}G\Sigma_g\left(\Sigma_g + \frac{\sigma_g}{\sigma_{s,z}}\Sigma_s\right), \tag{15}$$

where $\sigma_{s,z}$ can be calculated using Eq. 5. Although L08 found that P_h is not as good of a predictor of R_{mol} as the stellar surface mass density, it has a more solid physical basis (Wong & Blitz 2002; Blitz & Rosolowsky 2004, 2006; Elmegreen 1989; Elmegreen & Parravano 1994).

Another physically intuitive model is described by Krumholz et al. (2008, 2009a,b, hereafter KR relation or $R_{\mathrm{mol,K}}$) and tested by Krumholz & Gnedin (2011) using numerical simulations. In this model the molecular gas can only exist in a region well shielded from the UV radiation field. The approximate solution is

$$R_{\mathrm{mol,K}} = \frac{4 - 2s}{3s}, \tag{16}$$

(Krumholz & Gnedin 2011), where

$$s = \frac{ln(1 + 0.6\chi + 0.01\chi^2)}{0.6\tau_c}, \tag{17}$$

and where χ is a dimensionless number representing the scaled radiation field,

$$\tau_c = \Sigma_g a_d / \mu_H, \tag{18}$$

where a_d is the dust cross section per hydrogen atom and $\mu_H = 2.3 \times 10^{-24} g$ is the mean mass per nucleus. Following Krumholz & Gnedin (2011), we take the approximation that

$$\frac{\sigma_d}{10^{-21} cm^{-2}} = Z', \tag{19}$$

and

$$\chi \approx 3.1 \left(\frac{1 + 3.1 Z'^{0.365}}{4.1} \right), \tag{20}$$

with Z' being the metallicity normalised to the solar value. From Eq. 16 - 20 we expect some troublesome asymptotic behaviour in low density and low metallicity regions because a small τ_c ($\ll 0.5$) leads to a negative $R_{\mathrm{mol,K}}$. We therefore set negative $R_{\mathrm{mol,K}}$ values to zero in our code, which means there is no molecular gas in low density and low metallicity regions.

We test all three relations to estimate R_{mol} in our calculation (using the total gas surface mass density derived using our model, cf model description in section 3) and see which prescription best models the Σ_{HI} and $\Sigma_{\mathrm{H_2}}$ profiles.

2.3. Brief introduction to star formation laws

The SFL is usually defined as the relationship between star formation rate and ISM properties, especially density. The SFL allows one to calculate the star formation rate given

gas density and some other galactic parameters or vice versa. This is usually expressed as the surface density of star formation, Σ_{SFR}, defined as the SFR per unit area, or in other words the star formation intensity. There have been numerous SFLs and here we summarise and test the most popular ones in the literature (L08; Bigiel et al. 2008; Tan 2010, and references therein).

2.3.1. Schmidt-Kennicutt Law

Probably the most well known and widely used SFL is the Schmidt-Kennicutt Law (Schmidt 1959; Kennicutt 1998). It is a simple empirical correlation between star formation intensity and total gas:

$$\Sigma_{\mathrm{SFR,SK}} = A_{\mathrm{SK}} \left(\frac{\Sigma_g}{100 \mathrm{M}_\odot \, \mathrm{pc}^{-2}} \right)^N , \tag{21}$$

where A_{SK} is a coefficient with unit of $[\mathrm{M}_\odot \, \mathrm{kpc}^{-2} \, \mathrm{yr}^{-1}]$, Σ_g is the surface mass density of the gas (both neutral and molecular), and $N = 1.4 \pm 0.15$ (Kennicutt 1998). Here we fix $N = 1.4$ in our tests of $\Sigma_{\mathrm{SFR,SK}}$.

2.3.2. Free-fall time scale with fixed scale height

The power law index N of Schimidt-Kennicutt Law is very close to 1.5, which can be explained by arguing that stars form in a free-fall time scale in a gas disk with fixed scale height: Since the free fall time scale τ_{ff} is proportional to the inverse square root of the local gas density ρ_g, then for a fixed scale height h, the star formation intensity is (Leroy et al. 2008):

$$\Sigma_{\mathrm{SFR}} \propto \frac{\Sigma_g}{\tau_{\mathrm{ff}}} \propto \frac{\rho}{\rho^{-0.5}} \propto \Sigma_g^{1.5}. \tag{22}$$

Therefore the star formation intensity in a free-fall timescale with fixed scale height can be written as

$$\Sigma_{\mathrm{SFR,ff}} = A_{\mathrm{ff}} \left(\frac{\Sigma_g}{100 \mathrm{M}_\odot \, \mathrm{pc}^{-2}} \right)^{1.5} , \tag{23}$$

where A_{ff} has the same unit as A_{SK}. So this version of the SFL is nearly the same as the Schmidt-Kennicutt SFL with a slightly higher $N = 1.5$.

2.3.3. Free-fall timescale with variable scale height

If the disk scale height is not fixed but set by hydrostatic equilibrium, then the star formation law (still assuming stars form in disk free-fall time scale) is (Leroy et al. 2008)

$$\Sigma_{\mathrm{SFR,ff'}} = A'_{\mathrm{ff}} \left(\frac{\Sigma_g}{100 \mathrm{M}_\odot \, \mathrm{pc}^{-2}} \right)^2 \left(1 + \frac{\Sigma_s}{\Sigma_g} \frac{\sigma_g}{\sigma_{s,z}} \right)^{0.5} \left(\frac{11 km/s}{\sigma_g} \right), \tag{24}$$

where A'_{ff} has the same unit as A_{SK}.

2.3.4. Orbital timescale

If we instead assume that a constant fraction of the ISM is consumed in a dynamical timescale, we would have

$$\Sigma_{\mathrm{SFR,\Omega}} = B_\Omega \Sigma_g \Omega, \tag{25}$$

where B_Ω is a dimensionless coefficient and Ω is the orbital angular frequency (Leroy et al. 2008; Tan 2010). Following the suggestion of this functional form by Silk (1997) and Elmegreen (1997), Kennicutt (1998) showed that this form of the SFL was able to account for the star formation intensity in his sample of normal galaxies and circum-nuclear star burst, and worked equally well as $\Sigma_{\mathrm{SFR,SK}}$.

2.3.5. GMC collisions in a shearing disk

Tan (2000) presented a star formation model which assumes that star formation is triggered by GMC collisions in a shearing disk. This predicts that

$$\Sigma_{\mathrm{SFR,CC}} = B_{\mathrm{CC}} Q_g^{-1} \Omega (1 - 0.7\beta) \Sigma_g \quad (\beta \ll 1), \tag{26}$$

where B_{CC} is a dimensionless coefficient, $\beta \equiv d \ln v_{\mathrm{circ}} / d \ln r$ and v_{circ} is the circular velocity at a particular galactocentric radius r. Note $\beta = 0$ for a flat rotation curve. The GMC collision SFL is only meant to be valid in regions where a significant fraction of the gas is in gravitationally bound clouds, which typically means $\Sigma_{\mathrm{H_2}} \gtrsim \Sigma_{\mathrm{HI}}$. However, here we test it over a wider range of densities.

2.3.6. Linear molecular SFL

Leroy et al. (2008) and Bigiel et al. (2008) studied 12 nearby spiral galaxies at sub-kpc resolution and concluded that the SFR is proportional to the molecular content:

$$\Sigma_{\mathrm{SFR,H2}} = A_{\mathrm{H_2}} \left(\frac{\Sigma_{\mathrm{H_2}}}{100 \mathrm{M_\odot\, pc^{-2}}} \right), \tag{27}$$

where the coefficient $A_{\mathrm{H_2}}$ has the same unit as A_{SK}.

2.3.7. Turbulence-regulated SFL

Krumholz & McKee (2005) provided a turbulence-regulated star formation model to predict the SFR by assuming stars primarily form in molecular clouds that are virialised and supersonically turbulent and that the probability distribution of densities is lognormal. The intensity of star formation by their model is given by

$$\Sigma_{\mathrm{SFR,KM}} = A_{\mathrm{KM}} f_{\mathrm{GMC}} (\frac{\phi_{\bar{P}}}{6})^{0.34} (\frac{Q_g}{1.5})^{-1.32} (\frac{\Omega}{\mathrm{Myr^{-1}}})^{1.32} (\frac{\Sigma_g}{100 \mathrm{M_\odot\, pc^{-2}}})^{0.68}, \tag{28}$$

where the coefficient A_{KM} has the same unit as A_{SK}, f_{GMC} is the mass fraction of gas in giant molecular clouds (GMCs) and can be approximated as $f_{\mathrm{GMC}} = R_{\mathrm{mol}}/(1 + R_{\mathrm{mol}})$, and $\phi_{\bar{P}} = 10 - 8 f_{\mathrm{GMC}}$ (Krumholz & McKee 2005; Tan 2010).

2.3.8. Two-component SFL

Krumholz et al. (2009b) presented a two-component star formation law,

$$\Sigma_{\mathrm{SFR,KMT}} = A_{\mathrm{KMT}} f_{\mathrm{GMC}} \left(\frac{\Sigma_g}{100 \mathrm{M_\odot\, pc^{-2}}} \right) \times \left\{ \begin{array}{ll} (\Sigma_g/\Sigma_0)^{-0.33}, & \Sigma_g < \Sigma_0 \\ (\Sigma_g/\Sigma_0)^{0.33}, & \Sigma_g > \Sigma_0 \end{array} \right\}, \tag{29}$$

where the coefficient A_{KMT} has the same unit as A_{SK}, and $\Sigma_0 = 85 \mathrm{\, M_\odot pc^{-2}}$ is a 'critical' gas surface mass density. In regions with $\Sigma_g < \Sigma_0$, GMCs have an internal pressure that far exceeds the ambient gas pressure and the star formation time scale is independent of the environment; whilst in regions with $\Sigma_g > \Sigma_0$, the star formation time scale depends on the metallicity and the clumping.

3. The Model

Our model requires at least three inputs: the rotation curve, gas velocity dispersion and the stellar mass distribution. The metallicity is also needed if using the KR relation (cf. 2.2). The basic assumption for our model is that the galactic disk is in a gravitationally marginal stable state and the R_{mol} relations and SFLs are valid for all the galaxies.

Our algorithm is as follows:

1). Determine the radial total gas distribution ($\Sigma_g(r)$) assuming a marginally stable disk.

We make the assumption that the two-fluid stability parameter, $Q_{2\mathrm{f}}$, is constant through out the whole galactic disk. We test all four two-fluid stability parameters (Q_{R}, Q_{WS}, $Q_{\mathrm{RW,thin}}$, $Q_{\mathrm{RW,thick}}$, cf section 2.1) on our sample galaxies and pick out the one most suitable for our model and then adopt it for all further calculations. We define 'most suitable' in the first place as having the flattest Q profile with the smallest rms deviation over all or most of the sample galaxies, and as a secondary consideration the simplest form.

Based on eq. (1)-(12), we calculate the gas surface mass density Σ_g from the rotation curve $v(r)$, gas velocity dispersion and stellar surface mass density Σ_s by fixing the stability parameter $Q_{2\mathrm{f}}$ to the average value at intermediate radii.

2). Determine the radial molecular ($\Sigma_{\mathrm{H_2}}(r)$) and neutral ($\Sigma_{\mathrm{HI}}(r)$) gas distribution

We test three different ways to determine R_{mol}: the SR, PR and KR relations (cf. section 2.2). Once we have R_{mol} we determine the molecular gas surface mass density based on our model predicted Σ_g from step 1

$$\Sigma_{\mathrm{H_2}} = \Sigma_g \frac{R_{\mathrm{mol}}}{1 + R_{\mathrm{mol}}}, \tag{30}$$

and neutral gas surface mass density

$$\Sigma_{\mathrm{HI}} = \Sigma_g \frac{1}{1 + R_{\mathrm{mol}}}. \tag{31}$$

We then compare the derived molecular and neutral gas surface mass density to the observations to determine which R_{mol} relation fits the data best.

3). Determine the star formation intensity ($\Sigma_{\mathrm{SFR}}(r)$)

After obtaining the Σ_{HI} and $\Sigma_{\mathrm{H_2}}$, we use the SFL(s) introduced in section 2.3 to calculate the star formation intensity Σ_{SFR}. Following Tan (2010), we fit each galaxy using every SFL described in section 2.3. The results are evaluated to determine which SFL(s) fit the observed Σ_{SFR} best so as to implement in future application of our model.

4. The Data

In order to construct our model, we need the following quantities as inputs: the rotation curve $v(r)$, the stellar surface mass density Σ_s, the gas velocity dispersion σ_g, and metallicity. Also, for comparison with the observations, we need data for the neutral gas surface mass density Σ_{HI}, the molecular gas surface mass density Σ_{H_2} and the star formation intensity Σ_{SFR}.

The best sample, which has all the data listed above, is a subset of the THINGS sample (L08; de Blok et al. 2008). It is composed of five dwarf galaxies (DDO 154, IC 2574, NGC 7793, NGC 2403, and NGC 925) and seven spiral galaxies (NGC 3198, NGC 4736, NGC 6946, NGC 3521, NGC 5055, NGC 2841, and NGC 7331). The Σ_s, Σ_{HI} and Σ_{H_2} are tabulated in the paper of L08, although the dwarf galaxies do not have CO data and thus do not have Σ_{H_2}. The $v(r)$ is provided by de Blok et al. (2008).

L08 used a fixed value of $\sigma_g(= 11 km/s)$. However, in general σ_g is observed to vary in galaxies (Tamburro et al. 2009; O'Brien et al. 2010). Therefore, we tried both the measured σ_g and a fixed $\sigma_g = 11\,\text{km/s}$ when calculating the Q_{2f}. The measured σ_g are from A. C. Primo & F. Walter (private communication) and plotted in Fig. 3

The metallicity data is taken from Moustakas et al. (2010). We use a linear fit for each galaxy based on its metallicity zero point and radial gradient (Kobulnicky & Kewley 2004) provided by Moustakas (private communication). The solar metallicity is taken as $12 + \log(\text{O/H}) = 8.69$ (Moustakas et al. 2010; Asplund et al. 2009).

For the rotation curve $v(r)$, we fit the data using the universal rotation curve (URC) (Battaner & Florido 2000; Persic et al. 1996). The URC can be parameterised as

$$v^2(r) = v_0^2 \beta \frac{1.97 x^{1.22}}{(x^2 + 0.78^2)^{1.43}} + v_0^2 (1 - \beta)(1 + a^2)\frac{x^2}{x^2 + a^2}, \tag{32}$$

where $x = r/r_{opt}$ is the radial variable. Nominally, r_{opt} is the radius encircling 83% of the light, v_0 is the velocity at $r = r_{opt}$, while β and a are constants that depend on the luminosity. Here we keep the v_0, r_{opt}, β, and a as free parameters.

The rotation curve data and their URC fits are shown in Fig. 1. The main advantage of using such a smooth rotation curve fit is to have a well defined and realistic derivative of $v(r)$. This is important when calculating κ (eq. 2) and thus essential for any version of Q_{2f}. We note that an overly tight fit to all the kinks and wiggles in the rotation curve amplifies these features in the derivative, producing unrealistic results, especially when the fitted $v(r)$ profile declines faster than Keplerian. It is likely that these small amplitude variations in $v(r)$ result from noise in the data and small scale non-circular motions due to bars, spiral

arms, and asymmetries.

The URC parameters are fitted using the `MPFIT` software package (Markwardt 2009) to $v(r)$. We also tried two other rotation curve parameterisations: the exponential form (L08) and the arctan form (Courteau 1997). Generally, the URC model fits the data best, therefore we use the URC fit for all the rotation curves in this paper. The URC model fitting sometimes results in unphysical parameters (e.g. the fitted R_{opt} of DDO 154 is 12.1 kpc, far greater than the observation, 1.2 kpc; L08), but we use them anyway because we are only concerned with getting a smooth form which can best represent the data.

5. Results

5.1. The two-fluid stability parameter $Q_{2\mathrm{f}}$

The four two-fluid Q models are fitted to a constant (in forms of $\log Q$) using the `MPFIT` software package. In order to assess the quality of the fit we use the "deviation value" ϵ_Q which we define as

$$\epsilon_Q = \sqrt{\frac{1}{N_{\mathrm{ann}} - 1} \sum_{i=1}^{N_{\mathrm{ann}}} \left(\log \frac{Q_{\mathrm{model}}}{Q_{\mathrm{obs}}} \right)^2}, \tag{33}$$

where N_{ann} is the number of valid annuli in the galaxy. ϵ_Q has units of dex; values of ϵ_Q closest to zero indicate the model that most closely represents the observations. The fitted values and their corresponding deviation values are shown in Table 1. Because the observed $Q_{2\mathrm{f}}$ are less constant in the central and outer regions, we only use the data within the intermediate disk during the fitting. In terms of flatness, the average ϵ_Q listed at the bottom of the Table 1 indicate that Q_{R} is marginally the best recipe, followed by $Q_{\mathrm{RW,thick}}$, Q_{WS}, and $Q_{\mathrm{RW,thin}}$. It is satisfying that the form of $Q_{2\mathrm{f}}$ that is most rigorously defined yields the lowest average ϵ_Q, because it suggests that the feedback processes are truly working to maintain disks at a constant stability, at least over the intermediate radii. But since all these $Q_{2\mathrm{f}}$ recipes result in typically a factor of ~ 1.6 deviations about the mean, we choose to use Q_{WS} in our calculations as the easiest to implement, and sufficient for our purposes.

Figure 2 shows Q_{WS} for each galaxy using two cases for the gas velocity dispersion: a fixed $\sigma_g (=11\mathrm{km/s}; \mathrm{L08})$ and the measured σ_g. Apparently, there is little difference in these two situations. Furthermore, we calculate the σ_g needed to maintain a constant Q_{WS} and plot it on top of the measured σ_g in Figure 3. In most cases or at nearly all radii, the needed σ_g is within 1σ uncertainty of the data and very close to a constant $\sigma_g = 11km/s$ as well. Therefore, in order to keep the simplicity of our model, we use the fixed $\sigma_g (= 11km/s)$ in the following calculations.
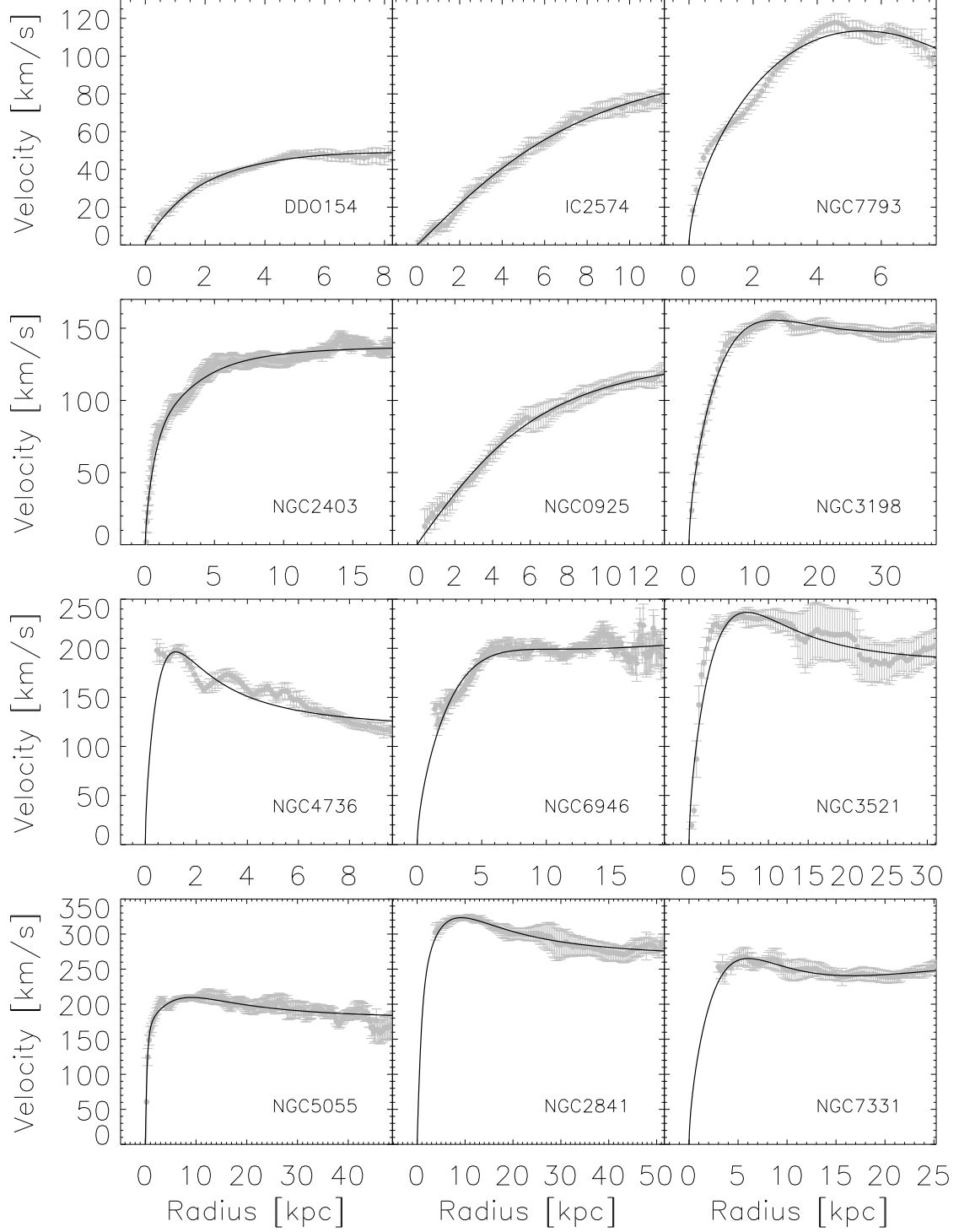
Fig. 1.— Rotation curve data and URC fitting. The grey dots with error bars are measured rotation curve data with uncertainty and the black solid lines are the URC fits.
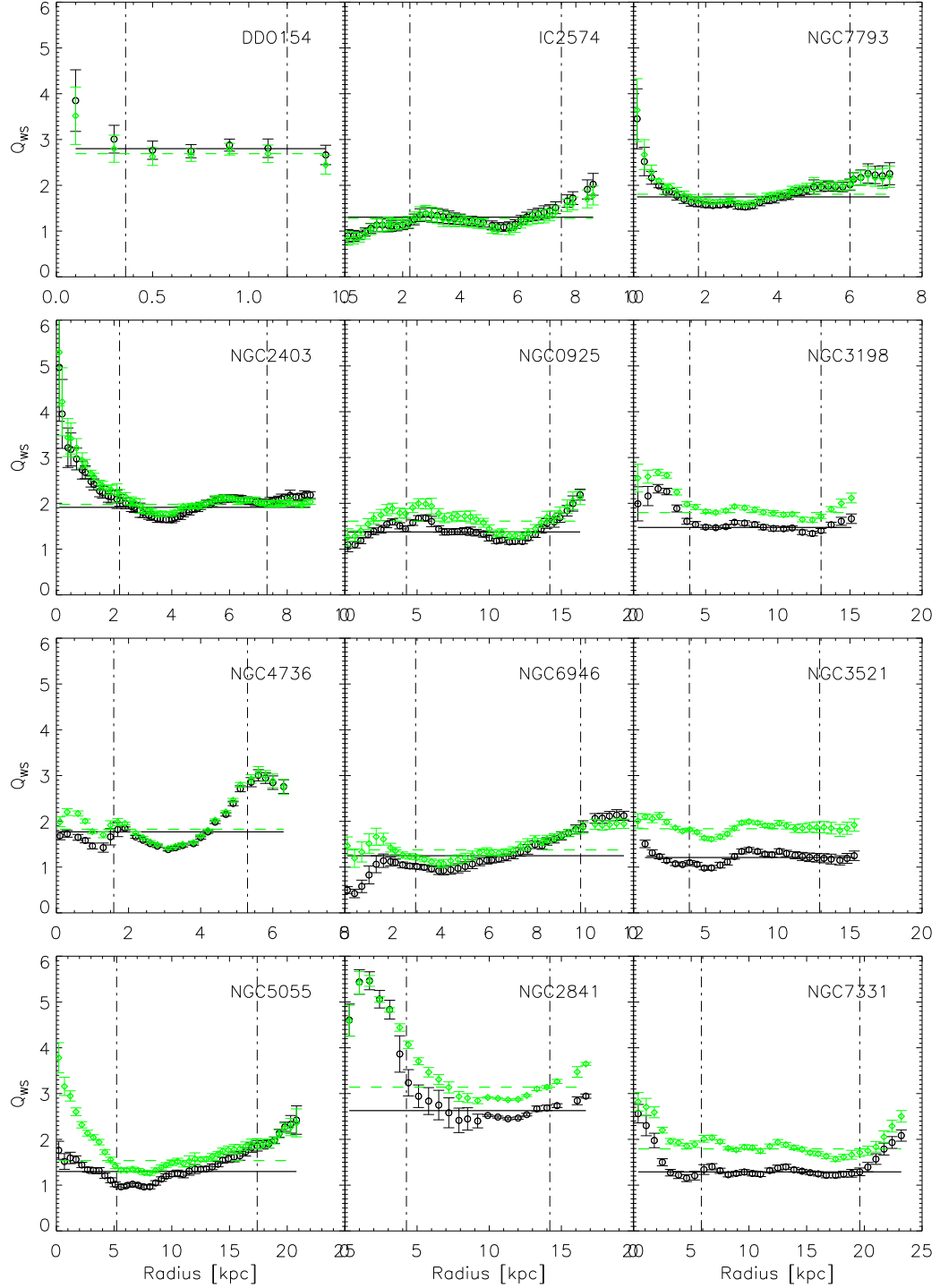
Fig. 2.— Q_{WS} radial profiles. Black open circles are Q_{WS} calculated using $\sigma_g = 11 km/s$ and black solid lines are their best constant fit; green open diamonds are Q_{WS} calculated using measured σ_g, and green dash lines are their best constant fit. Error bars show 1σ uncertainty.

5.2.   Neutral and molecular hydrogen content

We next calculate the neutral and molecular gas surface densities using the three R_{mol} relations: SR, PR and KR (cf. section 2.2). We use the fitted Q_{WS} values tabulated for each galaxy in Table 1 to derive the gas distribution. The calculated Σ_{HI} and $\Sigma_{\mathrm{H_2}}$ radial profiles are shown in Fig. 4 and Fig. 5 respectively. We calculate deviation values ϵ_{HI} and ϵ_{H2} for the three R_{mol} relations ($\epsilon_{\mathrm{HI,SR}}$, $\epsilon_{\mathrm{HI,PR}}$, etc.) using equations analogous to Eq. 33 to compare how well the Σ_{HI}, and the $\Sigma_{\mathrm{H_2}}$ observations and model agree. A cursory comparison of Fig. 4 with Fig. 5 suggests that the HI profiles do not fit the data as well as the H_2 profiles. However, this is largely illusory - the Σ_{HI} profiles are much flatter than the $\Sigma_{\mathrm{H_2}}$ profiles for which a larger display range is required. Comparison of the ϵ_{HI} and $\epsilon_{\mathrm{H_2}}$ values in Table 2 demonstrate that in general the HI profiles are fit by the model about as well or better than the H_2 profiles. All three R_{mol} model predictions agree with the data (cf. Table 2) reasonably well with the average $\epsilon_{\mathrm{HI}} \leq 0.19$ and the average $\epsilon_{\mathrm{H2}} \leq 0.29$, equivalent to fractional errors better than 0.6 and 0.9 respectively. The KR relation is the best in terms of the ϵ_{HI} values and the SR relation is the best in terms of $\epsilon_{\mathrm{H_2}}$ values. However, in some low metallicity regions and/or galaxies (e.g. DDO 154 and IC 2547) the KR relation results in no molecular gas. We do sometimes have a very bad fit (e.g. Σ_{HI} of NGC 2841) or even failure (e.g. Σ_{HI} of NGC 4736). The failure is caused by the big dip in the measured Q_{WS} curve (Fig. 2) which means the disk is already nearly unstable from just the stars.

The predicted HI surface mass density is usually flat over the radii considered here, but the model sometimes has a big divergence from the data in the outer regions where the observed HI has a steep decline, e.g. in NGC 925 and NGC 6946.

Note that the R_{mol} relations are tested using our CQ-disk model predicted Σ_{g}, not the observed total gas surface mass density. The best R_{mol} relation we find here need not necessarily be the best one would find when applying to observed ISM profiles. However, our results are consistent with those of L08, who found the SR relation best in determining the molecular contents using observed values.

5.3.   Star formation rate

Following Tan (2010), we test all SFLs introduced in section 2.3 using the derived Σ_{HI} and $\Sigma_{\mathrm{H_2}}$ (cf. section 5.2) as the input gas surface mass density values. For each galaxy, we derive the best-fit coefficients (e.g. A_{SK}, B_{Ω}, etc.) for these SFLs and measure the resultant uncertainty, ϵ_{SFR}, which is defined in a similar way to Eq. 33. Since we have three different R_{mol} models, we also have three different sets of Σ_{HI} and $\Sigma_{\mathrm{H_2}}$ (cf. section 5.2) and therefore
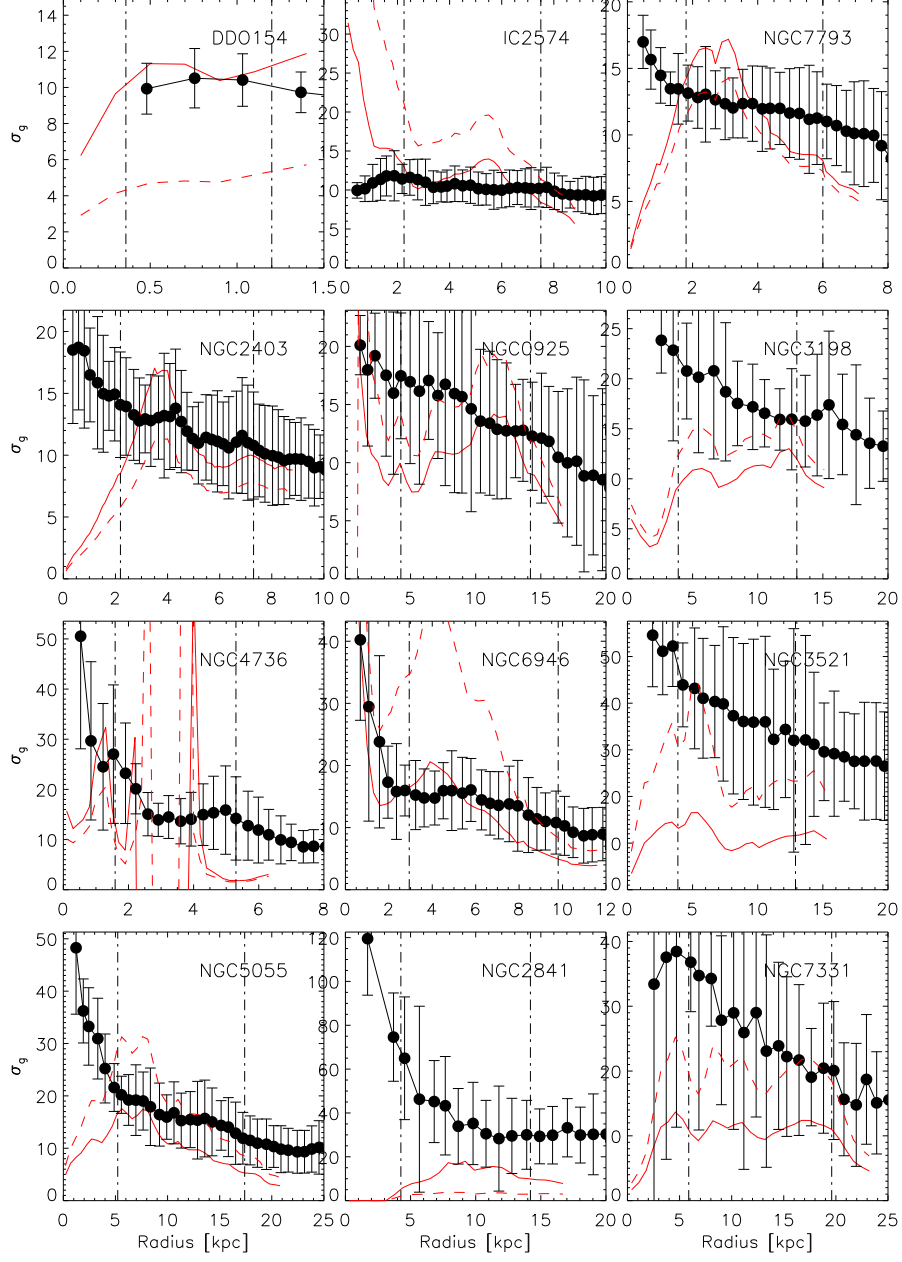
Fig. 3.— Gas velocity dispersion σ_g needed in order to keep a constant $Q_{\rm WS}$ with observed rotation curve and Σ_g and Σ_s. Red solid and dashed lines are the needed gas velocity dispersion calculated using the average $Q_{\rm 2f}$ value for the particular galaxy from Table 1 and a fixed $Q_{\rm WS} = 1.65$ respectively. Measured gas velocity dispersion with 1σ uncertainty are also over-plotted as black dots and error bars. The σ_g data are from Primo & Walter (private communication).
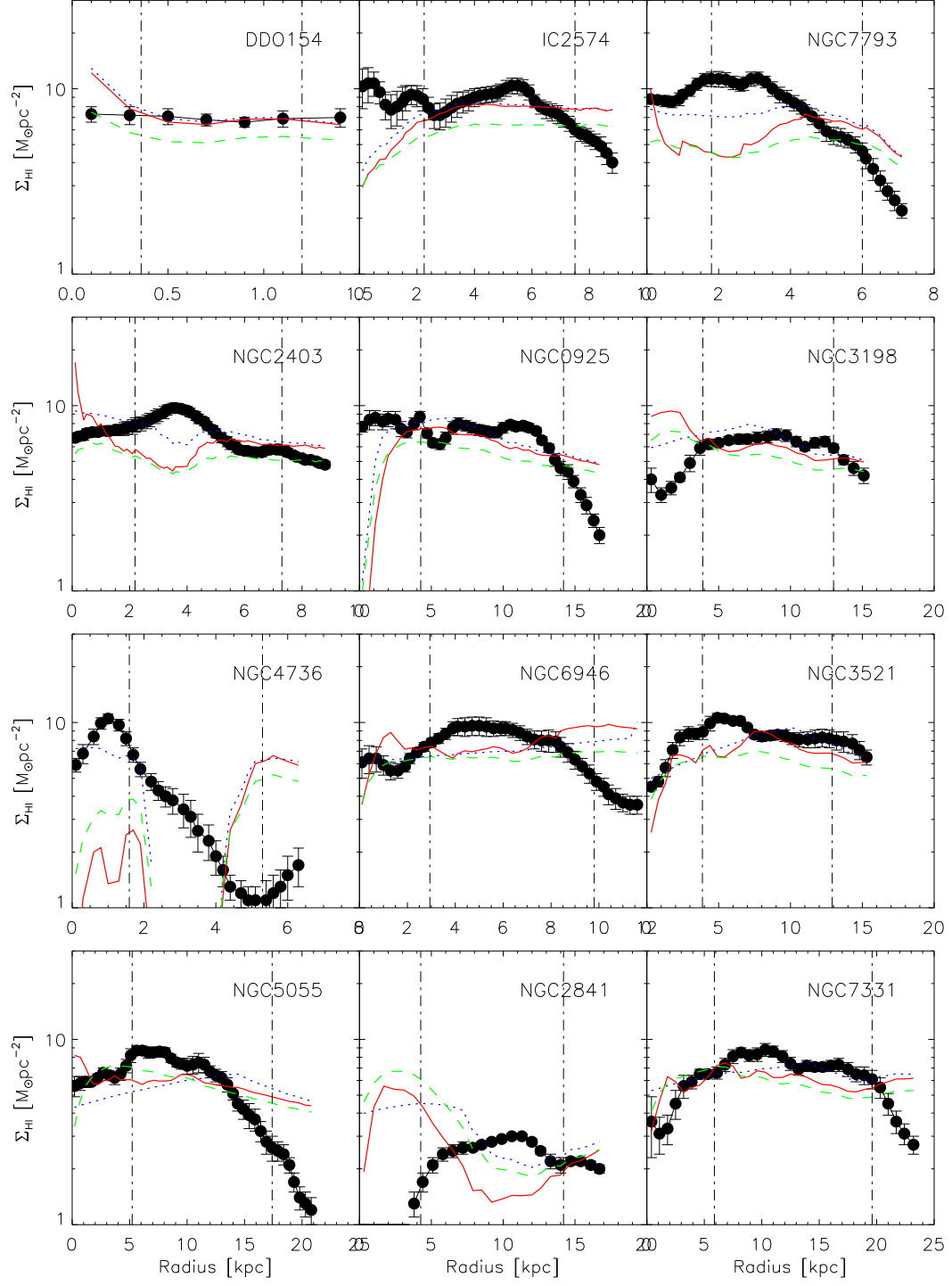
Fig. 4.— The Σ_{HI} radial profiles. Black dots and error bars are measured data with 1σ uncertainty; and red solid, green dash and blue dot lines are model derived Σ_{HI} using SR, PR and KR R_{mol} relations (cf. section 2.2) respectively.
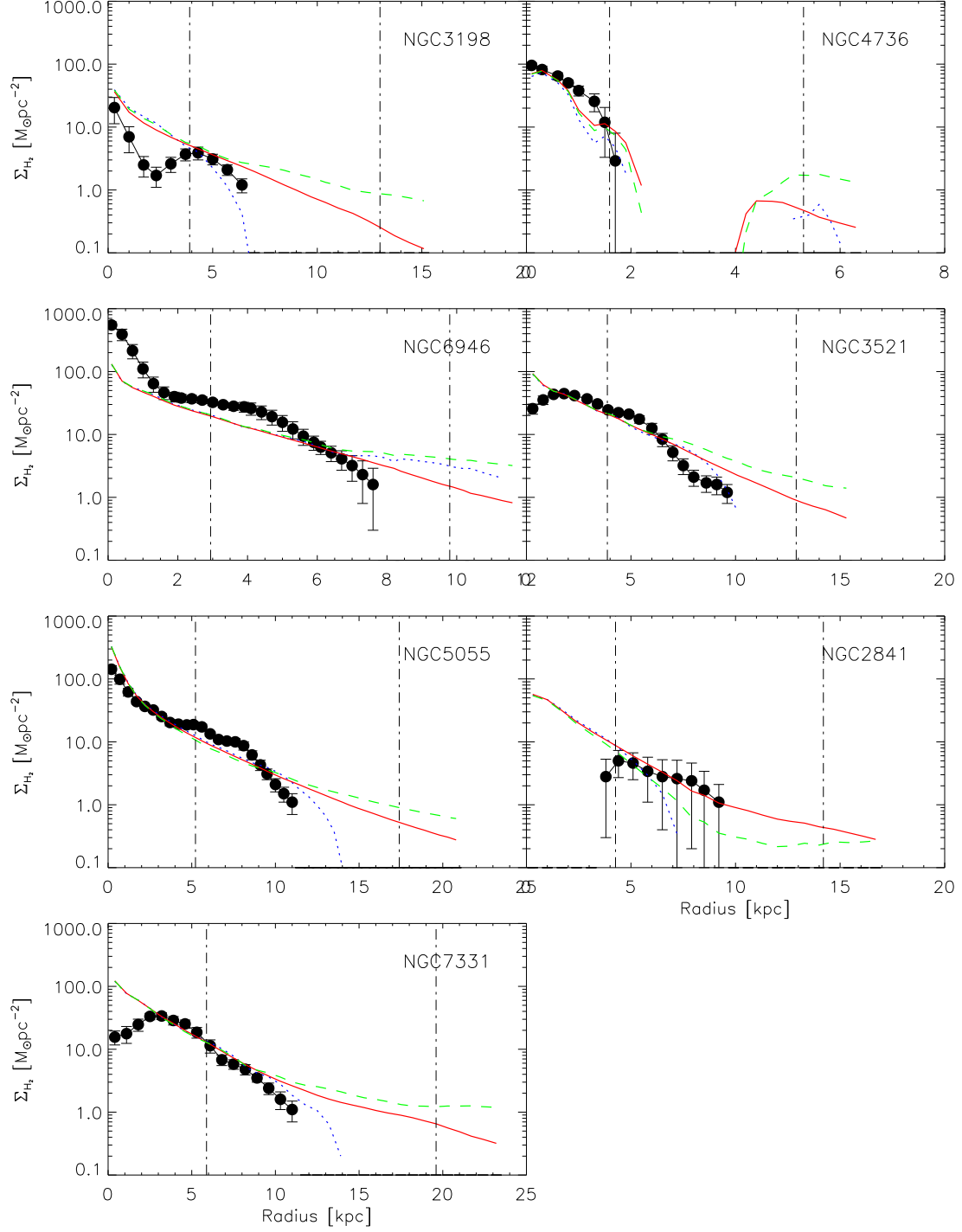
Fig. 5.— The Σ_{H2} radial profiles. Conventions follow Fig.4. There are only 7 galaxies shown here because we do not have CO data for the other 5 galaxies.

three different fitted SFL coefficients.The coefficients and the corresponding ϵ values are listed in Table 3 and 4. The resulting Σ_{SFR} profiles from the SFLs are plotted on top of the observed data in Figs. 6, 7, and 8.

Comparing the curves in Fig. 6, 7, and 8 the SFLs that depend on separating the molecular and neutral phases generally fit better than the SFLs that just depend on the total cool and cold ISM content. The predictions based on the SR relation performs better than PR and KR relations in terms of SFR predictions. The KR relation generally performs the worse in terms of SFR predictions. In addition, we see from Table 4 that the coefficient of the fit strongly correlates with stellar mass (as seen in the ordering of the table rows) when using the KR prescription for R_{mol}. This means that SFL with this prescription is not universal. The ϵ_{SFL} values in Tables 3 and 4 also support the view that the the molecular SFLs using the SR R_{mol} relation generally work the best. The exception to this rule is the dynamical time SFL (SFR$_\Omega$) which outperforms the turbulence regulated molecular SFL (SFR$_{\text{KM}}$) using the SR relation and all molecular SFLs using the PR and KR relation. However, the values in Tables 3 and 4 are the fit results using the intermediate radii data only. In terms of the simultaneous fit to all data points it is the third best SFL ($\epsilon_\Omega = 0.39$) following the linear molecular SFL (best, $\epsilon_{\text{H2}} = 0.30$) and the two component SFL (second best, $\epsilon_{\text{cc}} = 0.34$). This is slightly different from the results of Tan (2010) who found the two component (KMT) SFL to be the best SFL in terms of rms dispersion. The best fit to all data for the linear molecular SFL yields a coefficient $A_{\text{H}_2} = 9.51 \times 10^{-2}\,\text{M}_\odot\,\text{yr}^{-1}\,\text{kpc}^{-2}$ using the SR relation. This is slightly higher than the L08 value, $(5.25 \pm 2.5) \times 10^{-2}\,\text{M}_\odot\,\text{yr}^{-1}\,\text{kpc}^{-2}$, but well within its 2σ uncertainty. The higher coefficient implies 80% more efficient star formation and shorter molecular gas cycling times than those derived by L08.

Note that the GMC collision SFL is meant to be applied to molecular gas rich regions only (cf. section 2.3.5). It is therefore not surprising that our application of this SFL in regions that are not dominated by molecular gas, such as central region of NGC 2841, results in a poor match to the observed Σ_{SFR}. Once more, one should bear in mind that the best SFL is selected based on our model predicted gas contents (Σ_g or Σ_{H_2}). This is different from the standard approach of using the observed Σ_g or Σ_{H_2} to predict Σ_{SFR}. Most of the best-fit SFL coefficients (A or B coefficients in Table 3 and 4), except the coefficient of the GMC collision SFL (B_{CC}) and the coefficient of the KMT SFL (A_{KMT}), are on the order of but a little bit larger than those of Tan (2010), who apply the SFLs onto observed gas surface mass densities. Since we have slightly different sample galaxies with Tan (2010), it is possible to have very different fitting values, however in fact, we do have similar B_{CC} and A_{KMT} values to those of Tan (2010) for galaxies in the overlapping part of our and Tan's sample. The model-observation deviation (ϵ values in Table 3 & 4) have similar situation: they are also generally larger than but on the order of those in Tan (2010, the χ values).

For example, for the galaxy NGC 7331, we find $\epsilon_{\mathrm{SFR}} = 0.056$ for the linear molecular SFL while Tan (2010) determines $\epsilon_{\mathrm{SFR}} = 0.0493$ for this SFL. However, the combination of the SR prescription for R_{mol} and the linear molecular SFL is claimed to provide the best results by L08, which is consistent with our results.

6. Discussion

6.1. Variations in $Q_{2\mathrm{f}}$ and σ_g

The basic assumption of our model is that the two-fluid stability parameter $Q_{2\mathrm{f}}$ is a constant. As we can see from Fig. 2, Q_{WS} is roughly constant, especially at intermediate radii. The variation can be large, up to a factor of 3 over the whole radial range sampled but the variations within the intermediate radii regions are smaller, less than a factor ~ 1.5 except for three cases NGC4736, NGC 6946, and NGC5055, where the variations are a factor of ~ 2 (see Table 1). There is also systematic variations with galactocentric radius: in 7/12 cases Q_{WS} rises towards the centre, sometimes quite sharply (NGC7793, NGC2403, NGC5055, NGC2841), while in 3/4 of the sample Q_{WS} increases at large radii, mostly beyond r_{25}. This systematic variation may cause over prediction of gas and SFR surface densities in the central and outer regions. A rapid central rise of Q_{WS} can have several explanations, which are discussed in section 6.2. The slow rise of Q_{WS} beyond r_{25} might be caused by undetected molecular gas in the outer disk, or may be due to the limited supply of ISM as pointed out by Meurer et al. (2013).

The gas velocity dispersion is hard to measure (Tamburro et al. 2009) and has large uncertainties (cf. Fig. 3). However, as shown in Fig. 2 the shape of the Q_{WS} profiles is not greatly affected by choosing a constant σ_g or adopting the observed σ_g profiles. In four cases (NGC3198, NGC3521, NGC2841, and NGC7331) the profiles are noticeably shifted vertically between the two options. This is because the measured σ_g is significantly higher than the assumed value of 11 km s^{-1}. We can also see from Fig. 3 that the σ_g needed to keep a constant Q_{WS} (using the observed Σ_s and Σ_g in Eq. 1, 3 and 9) is pretty constant and close to 11km s^{-1} and well within 2σ uncertainty of the measured gas velocity dispersion.

It might be surprising that Q_{WS} does not vary much no matter whether we use a constant $\sigma_g = 11$kms^{-1} or the measured σ_g. This is because the definition of Q_{WS} (eq. 9) is similar to the equivalent resistance of two resistors connected in parallel and Q_s is usually smaller than Q_g in the inner and intermediate disk regions. Thus, Q_{WS} is usually dominated by the Q_s value. This also illustrates that it is the total stability parameter, $Q_{2\mathrm{f}}$, instead of Q_g that matters most and the interaction between gas and stars plays an important role in balancing
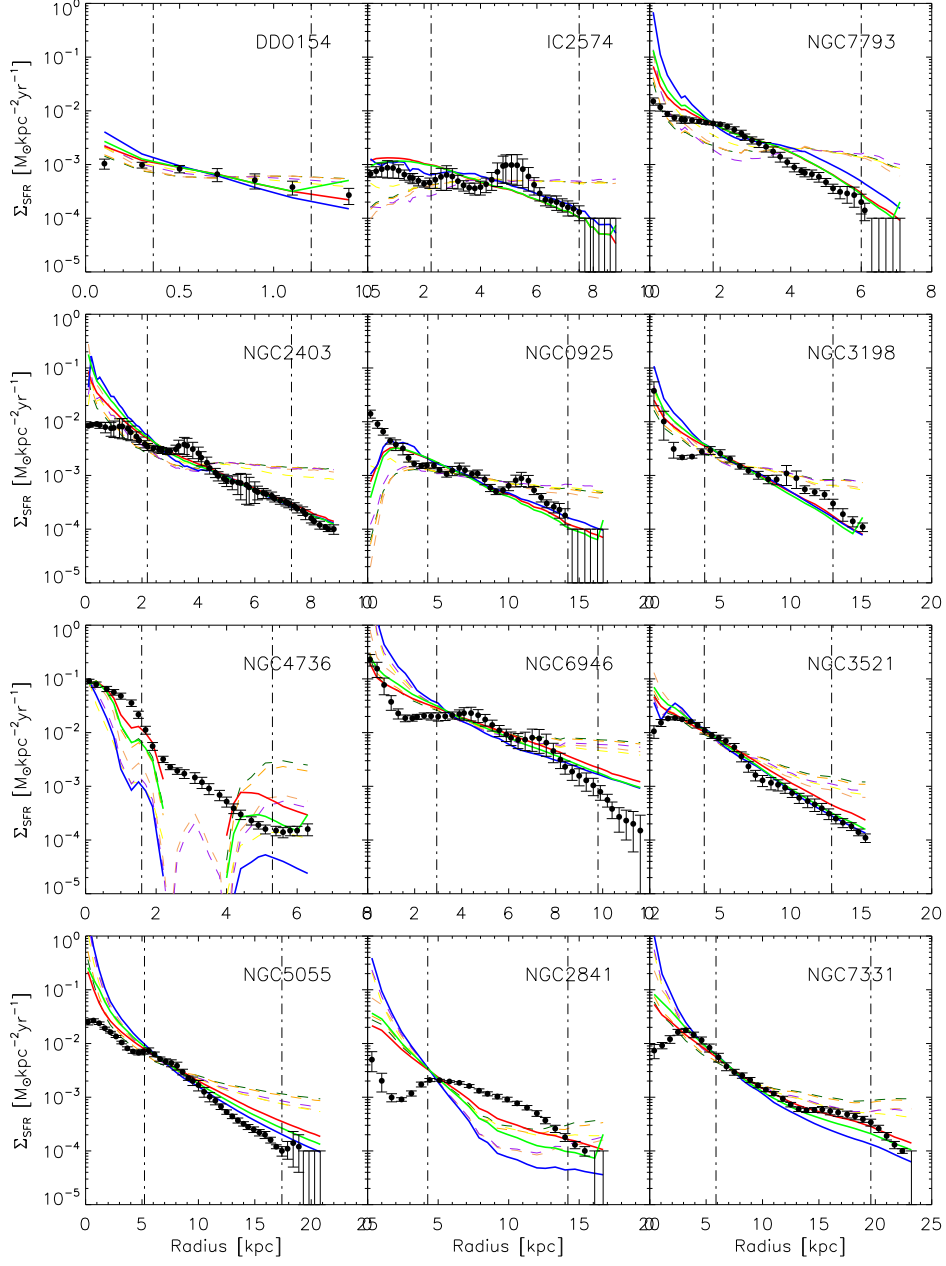
Fig. 6.— Σ_{SFR} radial profiles using the SR prescription for R_{mol}. Black dots and error bars are measured Σ_{SFR} from L08. Thick solid lines are the three best fit SFLs: red, linear molecular SFL; blue, turbulence regulated SFL; green, two-component SFL. Dash lines are other SFL predictions: dark green, SK law; orange, free-fall with fixed scale height; sandy brown, free-fall with variable scale height; yellow, orbital time scale; purple, GMC collision.
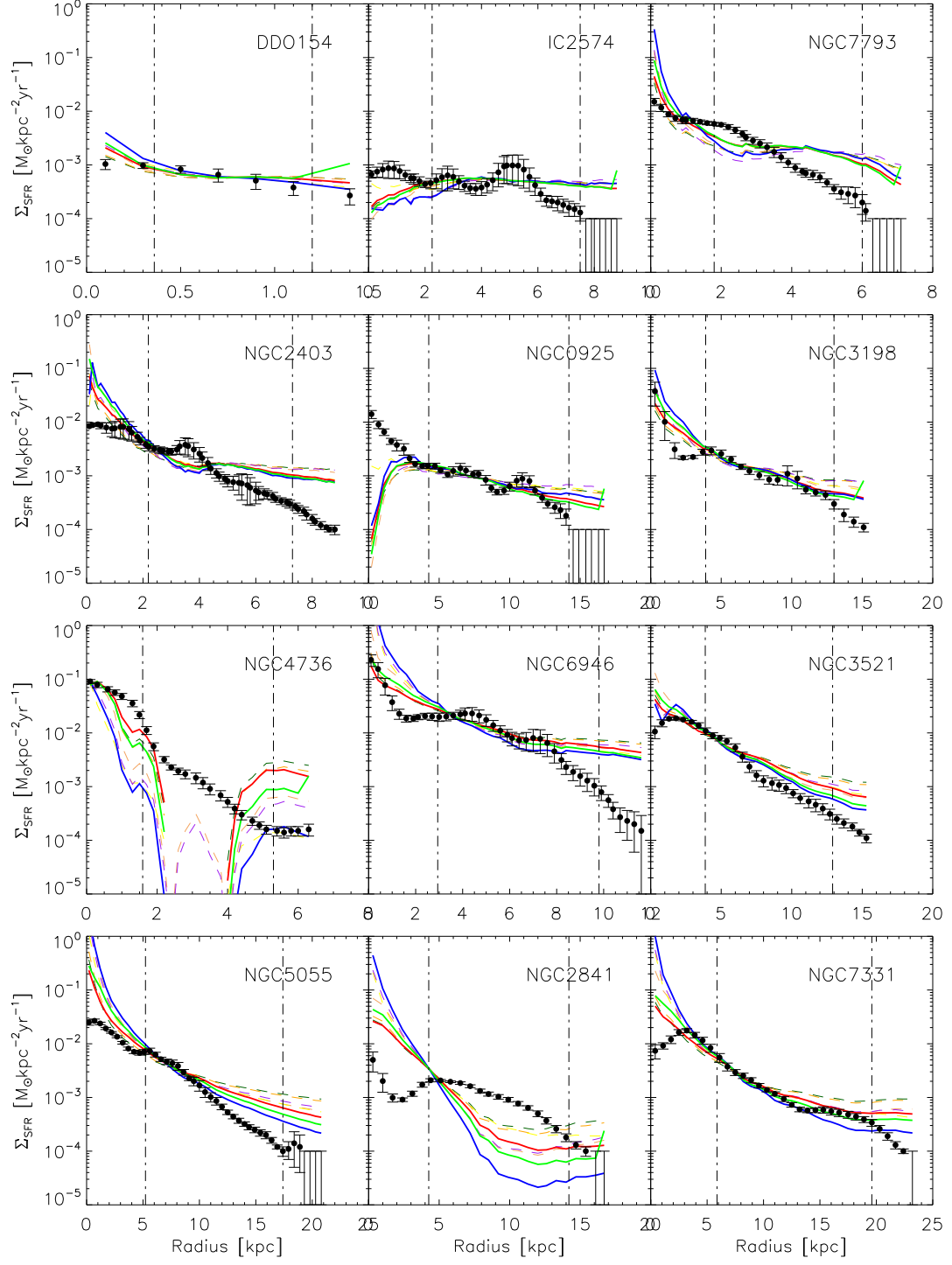
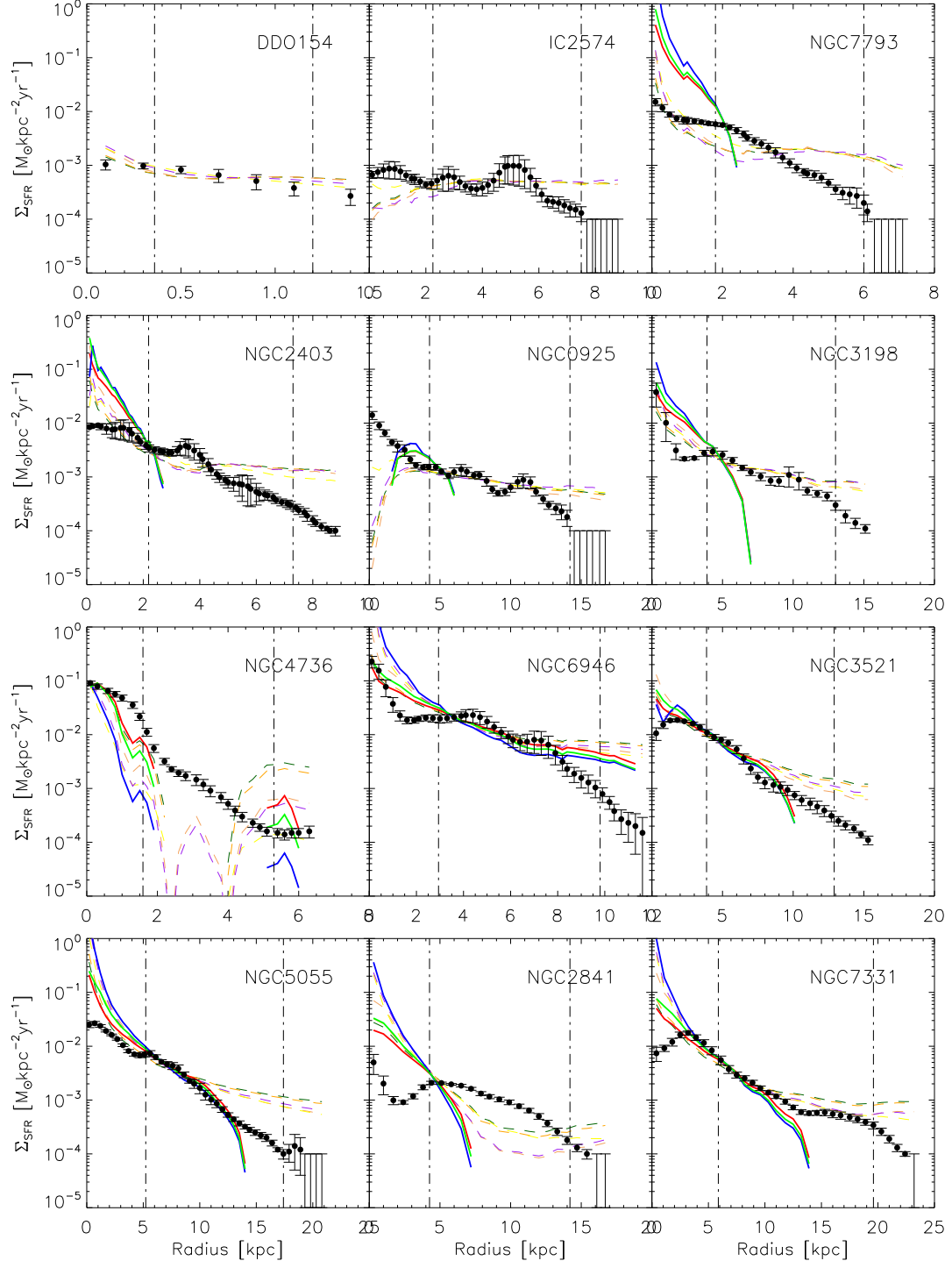Fig. 7.— $\Sigma_{\rm SFR}$ radial profiles using the PR prescription for $R_{\rm mol}$. Conventions follow Fig.6.

Fig. 8.— $\Sigma_{\rm SFR}$ radial profiles using the KR prescription for $R_{\rm mol}$. Conventions follow Fig.6.

the stability of galactic disk.

6.2.   The central disk

Figures 7 - 8, suggest that our model overestimates Σ_g and/or $\Sigma_{\rm SFR}$ in the central disk for many of the sample galaxies. In e.g. NGC 2841, NGC 2403 and NGC 7331, the model overestimates Σ_g and $\Sigma_{\rm SFR}$ by more than an order of magnitude. This result is similar to that of Quirk (1972) although he used a different stability criterion (Goldreich & Lynden-Bell 1965). Quirk (1972) argued that this is because the density-wave-induced shocks, which are very strong in the inner parts of the galaxy, make the gas in the post shock regions dense enough to be Jeans unstable. Thus their stability criteria, which does not consider shocks, may not be a good representation for the inner disk stability. However, our model does work well in the central part of other galaxies, e.g. NGC 7793, and furthermore, our model sometimes underestimates the central disk SFR of galaxies like NGC 6946 and NGC 925. Possible reasons for the model-observation discrepancy in the central disk could be the fitted functional form of the rotation curves are not good enough to represent the data (cf. section 6.3), or the central disk is not a suitable place to apply our model because it is dominated by a bulge instead of being pure disk.

Despite these complications and the poor fit to the central region in detail, Fig. 9 shows that the SFR integrated over the central region from our model agrees with the data to a similar level of accuracy as it does over the intermediate radii. The specific model we are using here employs the $Q_{\rm WS}$ recipe for $Q_{\rm 2f}$, the SR formulation of $R_{\rm mol}$, and the linear molecular SFL $\Sigma_{\rm SFR,H2}$. The relatively good agreement in the central region is because usually the model only fails badly in the very central part of the disk, typically covering an area less than 50% of the central disk. Therefore, the integrated SFR does not deviate from the observation very much. The exception to this is NGC 2841, where the modelled SFR profiles shown in Figs. 6 - 8 deviate strongly from the observed over the entire central disk.

6.3.   Effects of rotation curve parameterisation

Since Q is dependent on the derivative of the rotation curve (through κ), the precise shape of the smooth fit must have a quite strong effect on the result, especially in the inner region, where the rotation curve rises rapidly. In order to test this effect, we use the exponential parameterisation to fit the RC of NGC 2403 and use these new fitting results to recalculate the gas and star formation distribution. The results are shown in Fig. 10. The
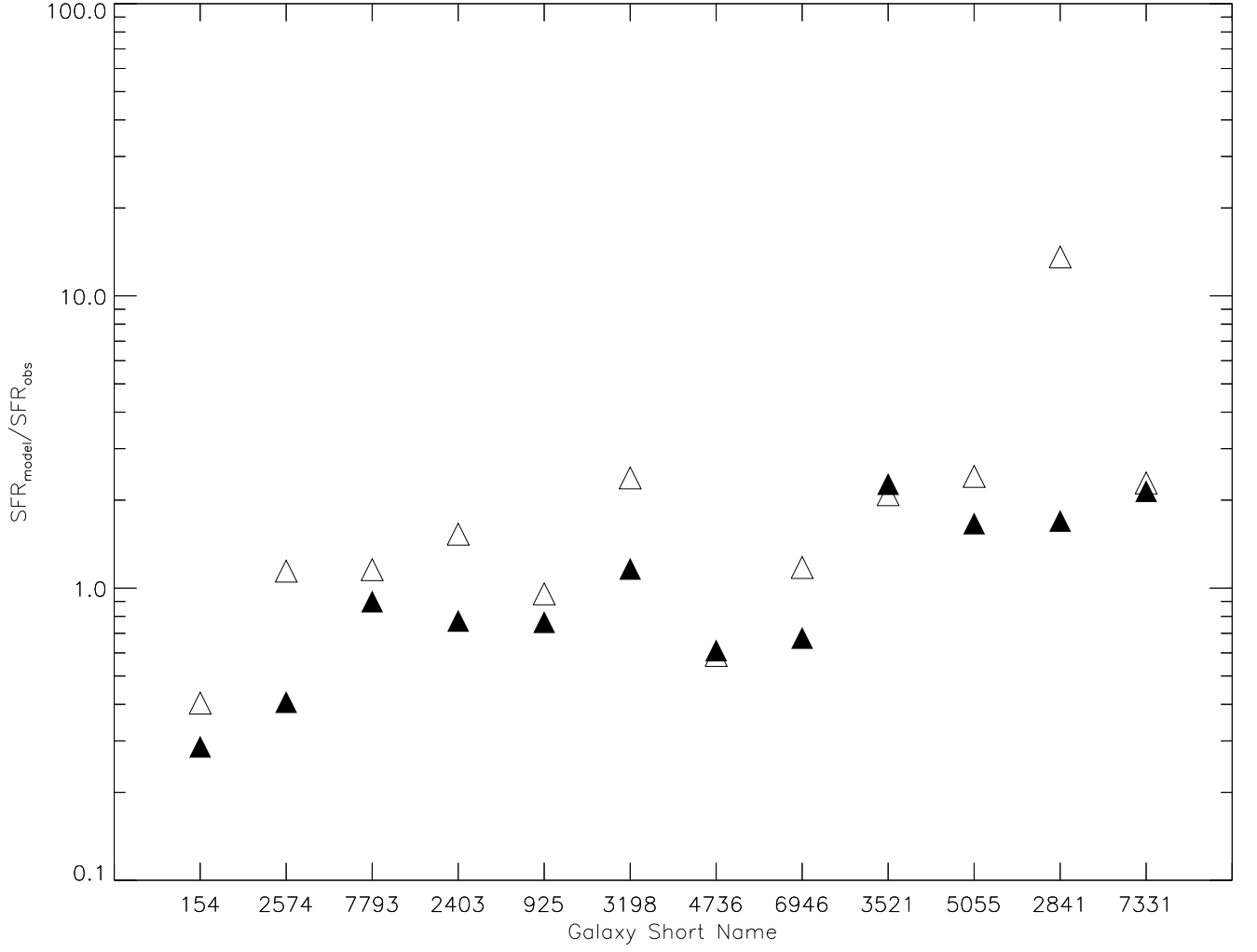
Fig. 9.— The ratio of $SFR_{\mathrm{model}}/SFR_{\mathrm{obs}}$. Solid symbols are for intermediate disk and open symbols are for central disk. The specific model we are using here is the Q_{WS} recipe for Q_{2f}, the SR formulation of R_{mol}, and the linear molecular SFL $\Sigma_{\mathrm{SFR,H2}}$.

exponential form results in a shallower slope in the rising part of the RC and therefore a lowered gas and star formation surface density in the central region compared to the result of the URC fitting; whilst the URC form fitting results in a steeper slope and thus a higher gas and star formation surface density in the central region. As expected, different forms of RC fittings make little difference in the middle and outer disk for galaxies with a flat RC.

7. Tests and applications of the CQ-disk model

Examination of Figs. 4 – 8 and Tables 2 - 4 demonstrate that the CQ-disk model does a reasonable job (factor of ~ 2 agreement) of matching the overall shape of the H$\textsc{i}$, CO, and SFR radial profiles especially at intermediate radii. Figure 2 indicates that these radii are where Q_{2f} is not only fairly flat but at its minimum, i.e. the most unstable but uniformly so. This may be because at these radii star formation feedback is effective and the timescales for ISM flows are sufficient for profiles to evolve to nearly constant stability. As emphasised in sec 6.2, the model has the most difficulties fitting the detailed profiles in the central regions of galaxies, but still is fairly reasonable in predicting quantities integrated out to $r = 0.3r_{25}$.

Even at intermediate radii, the model curves do not match the profiles in close detail, with the observed profiles having small scale bumps, dips, and kinks. Often these local enhancements can also be seen in the profiles of Q_{2f}, HI, H$_2$, and SFR (e.g. the kinks in the profiles in IC 2574 and NGC 3521 at $R \sim 5.5$ kpc). These indicate that local enhancements in the gas density are reflected in the SFR profiles as expected by any reasonable SFL, but result in the Q profiles not being flat in detail. While disks may be evolving towards a uniform stability, local deviations may build up due to processes beyond the scope of this model (e.g. internal resonances, external perturbations, minor mergers). Hence the CQ-disk model is not as well suited to modelling the details of individual galaxies as the overall structure of galaxies in general.

Our sample is relatively small. Further high quality observations would be useful to further test and optimise our model. New and developing generations of instrumentation including the JVLA, ASKAP, MeerKAT, Westerbork+APERTIF for H$\textsc{i}$ observations, ALMA, CARMA, and SMA for CO (and thus H$_2$), WISE, PanSTARRS, LSST for modelling stellar content, combined with star formation surveys such as HAGS (James et al. 2004), SINGG (Meurer et al. 2006), and 11HUGS (Kennicutt et al. 2008) as well as the wide availability of images of star formation from GALEX and WISE data mean that it will be possible to do studies similar to ours for well selected samples of hundreds or thousands of galaxies in the near future.
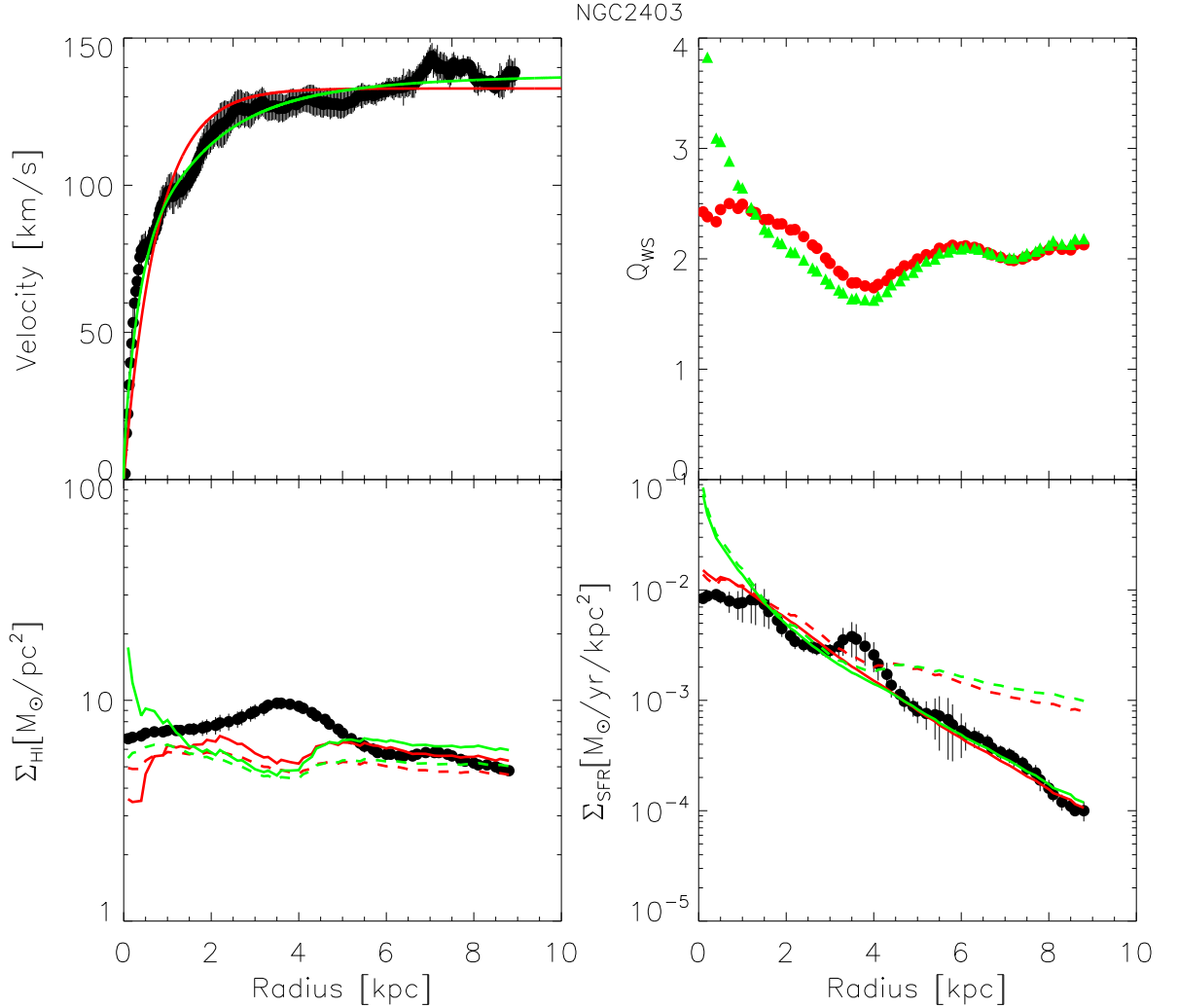
NGC2403

Fig. 10.— The effects on the results for NGC 2403 from using different rotation curve fitting functions. Upper-left panel: Rotation curve. Black dots with error bars are rotation curve data and uncertainties, the red solid line is the URC fit and the green solid line is the exponential rotation curve fit. Upper-right panel: Two-fluid stability parameter, Q_{WS}. Red dots are calculated using the fitted URC form and green triangles are calculated using fitted exponential rotation curve. Lower-left panel is HI surface mass density and lower-right panel is SFR surface density. In these panels the black dots with error bars are measured data with uncertainties. The red lines are calculated using the fitted URC rotation curve and green lines are calculated using the fitted exponential rotation curve, in both cases the appropriate constant Q_{WS} is adopted. Solid lines are results using the SR prescription for R_{mol} and dash lines use the PR prescription. The SFL used here is the linear molecular SFL.

Examination of Figures 4 – 8 demonstrates that the various R_{mol} and SFL prescriptions diverge from each other the most in the outer and central regions of galaxies. For the reasons discussed in Sec. 6.2 the centre is more difficult to model. So we concentrate on how further study of LSB galaxies and outer disks may improve our model. The SR and PR recipes diverge from each other there because the former only depends on the stellar surface mass density, while the hydrostatic pressure used in the PR prescription becomes more dominated by gas. The metallicity dependence of the KR relation combined with the metallicity gradients typically seen in the bright parts of galaxies (Zaritskey et al. 1994; Kennicutt et al. 2003; Moustakas et al. 2010) will also drive a radial gradient compared to the SR and PR prescriptions. LSB regions are also important to test because of indications of low level star formation in extended UV disk galaxies (Thilker et al. 2005; Thilker et al. 2007) and H I dominated regions (Bigiel et al. 2010b). This low intensity star formation likely signifies IMF variations (Meurer et al. 2009; Lee et al. 2009; Hunter et al. 2010; Gunawardhana et al. 2011) which should be incorporated in future versions of a more comprehensive CQ-disk model.

Comparison of the integrated H I mass and star formation rate may provide a sensitive test of our model since Figures 4, and 6-8 show that H I and star formation are largely segregated in galaxies, and the divergent behaviour of the various model profiles suggests that the H I/SFR ratio is likely to be dependent on the R_{mol} and SFL prescriptions. We will test this using data from the SINGG and SUNGG star formation surveys (Zheng et al. 2013, in prep).

The CQ-disk model may prove useful in galaxy simulations. For example, currently when generating the initial distribution of particles for N body simulations of interacting galaxies one often creates disks with the same scale length for stars and gas (e.g. Johansson, et al. 2009; Bekki & Couch 2011) or giving the stellar disks exponential profiles with differing scale lengths (e.g. Lotz et al. 2008). Assuming a constant Q_{2f} disk provides alternative easy to implement initial conditions for detailed simulations of galaxies. One could also use the CQ-disk model to enhance semi-analytic cosmological simulations, i.e. in a manner similar to that done by (Duffy et al. 2012a; Duffy et al. 2012b) who modeled the detectability of galaxies in future H I surveys. A similar application of the CQ-disk model will allow better H I line profile models, as well as models of H_2 (CO), and star formation in the same volume.

8. Summary

We have developed a simple 'constant Q disk' (CQ-disk) model for predicting the distribution of ISM and star formation in galaxies based on the assumption that the two-fluid instability parameter (Q_{2f}) of the galactic disk is a constant. The model predicts the gas

surface mass density and star formation intensity given the rotation curve, stellar surface mass density and the gas velocity dispersion. In this paper we compared radial profiles of HI, and H_2 surface mass density and star formation intensity from a sample of 12 galaxies from L08. In order to optimise our model, we tried various prescriptions for calculating Q_{2f}, the ratio $R_{mol} = \Sigma_{H2}/\Sigma_{HI}$, and the star formation law (SFL). We find that

- The Q_{2f} profiles are fairly flat over the intermediate radii of the disk, with variations of a factor of ~ 1.6 about the mean, no matter which recipe of Q_{2f} is employed. The Rafikov (2001) formulation of Q_{2f} has the strongest physical basis of the recipes we tried, and also marginally the flattest Q_{2f} profiles. However it is the most difficult to implement since it requires the wavelength of the most unstable mode to be derived. The Wang & Silk (1994) approximation, is the most practical recipe for Q_{2f} in terms of its very simple form, and the one we have adopted in our model.

- We tested three prescriptions of R_{mol} by comparing the observed surface mass densities of neutral and molecular gas with our model predictions. All three prescriptions produce Σ_{HI} and Σ_{H_2} profiles that match the observed profiles with typical variations better than a factor of 2 about the mean. Overall, the empirical scaling of R_{mol} with stellar surface mass density (SR) proposed by Leroy et al. (2008) produces the best fits to both the Σ_{HI} and Σ_{H_2} profiles, and therefore we favor this model. While the Krumholz et al. (2008, 2009a,b) self-shielding prescription KR produces typically better matches to the Σ_{HI} profiles than the SR relation, the matches to the Σ_{H_2} profiles are worse. Although the best R_{mol} relation selected here is based on the predicted Σ_g from our CQ-disk model, it is consistent with the L08 results based on observed neutral and molecular ISM profiles.

- We tested eight versions of the SFL, five that depend on just the total ISM content (defined as combined neutral and molecular component) and three that require the ISM be separated in to neutral and molecular phases. The latter three were tested with all three prescriptions of R_{mol} that we trialled. The linear molecular SFL, SFR_{H2} produces the best matches to the Σ_{SFR} profiles when used with the SR R_{mol} relation, with the models typically agreeing with the observed profiles to within a factor of 2. The two-component SFL SFR_{KMT}, combined with the SR relation does second best with agreement to typically a factor of 2.2, while the orbital time SFL SFR_Ω, at third best in terms of ϵ_{SFR} value, is the best of the single component ISM SFLs with agreement to within a factor of 2.5 over the intermediate radii disk. Again, the best SFLs here are selected based on our model predicted Σ_g as well as Σ_{H_2}, not the observed gas surface mass densities. However, the results are consistent with those from L08

and Tan (2010) who do use observed ISM profiles for their tests. This consistency also supports our CQ-disk model in an indirect way.

- The modelled star formation intensity profiles (Figs 6, 7, 8) match the observations best at intermediate radii, and show the largest deviations in the central region (where $R <= 0.3R_{25}$). This suggest that a more elaborate model is needed to explain the ISM and gas distribution in the centres of galaxies, especially those with bulges or a steeply rising rotation curve. However, integrating the SFR over the entire central region area we find that the models agree with the observations within a factor of 3 in all but one case. This indicates the systematic discrepancy integrated over galaxy centres generally is not severe.

Since we are testing a model for the distribution of star formation and gas in galaxies that we base on inferences from THINGS team results, there is no surprise that our model works well for large portions of galaxies selected from the THINGS sample. Our future papers will test our model on galaxies selected independently.

One advantage of our models is that they are easy to calculate given the rotation curve and the distribution of stellar mass. This may prove to be a useful advantage in terms of implementation compared to more detailed models like that of Ostriker et al. (2010). However to handle the central regions, some reasonable modifications may be required, such as requiring gas and SFR to only be at $r > 0.3r_{25}$ for galaxies with v_{flat} above some fiducial value.

REFERENCES

Asplund, M., et al. 2009, ARA&A, 47, 481

Battaner, E., & Florido, E. 2000, FCPh, 21, 1

Bekki, K., & Couch, W.J. 2011, MNRAS, 415, 1783

Bell, E. F. 2002, ApJ, 581, 1013

Binney, J., & Tremaine, S., Galactic Dynamics, Princeton Univ. Press, 2008

Bigiel, F., et al. 2008, AJ, 136, 2846

Bigiel, F., et al. 2010a, ApJ, 720, L31

Bigiel, F., et al. 2010b, AJ, 140, 1194

Blitz, L., & Rosolowsky, E. 2006, ApJ, 612, L29

Blitz, L., & Rosolowsky, E. 2006, ApJ, 650, 933

Boissier, S., Prantzos, N., Boselli, A., & Gavazzi, G. 2003, MNRAS, 346, 1215

Bosma, A. 1981, AJ, 86, 1825

Burton, W. B., Elmegreen, B. G., & Genzel, R., The Galactic Interstellar Medium, Springer-Verlag Berlin Heidelberg, 1992

Calzetti, D., et al. 2007, ApJ, 666, 870

Courteau, S. 1997, AJ, 114, 2402

Davé, R., Finlator, K., & Oppenheimer, B. D. 2011, MNRAS, 416, 1354

de Blok, W. J. G., et al. 2008, AJ, 136, 2648

Dopita, M. A. & Ryder, S. D. 1994, ApJ, 430, 163

Duffy, A.R., Moss, A., Staveley-Smith, L. 2012a, PASA, 29, 202

Duffy, A. R. 2012b, MNRAS, 420, 2799

Dutton, A., 2009, MNRAS, 396, 121

Dutton, A. & van den Bosch, F. C., 2009, MNRAS, 396, 141

Dutton, A. & van den Bosch, F. C., 2011, arXiv:1108.0663

Elmegreen, B. G. 1989, ApJ, 338, 178

Elmegreen, B. G. 1993, ApJ, 411, 170

Elmegreen, B. G. 1997, RMxAC, 6, 165

Elmegreen, B.G., & Parravano, A. 1994, ApJ, 435, L121

Elmegreen, B. G. 2011, ApJ, 737, 10

Fall, S. M., & Efstathiou, G. 1980, MNRAS, 193, 189

Ferguson, A. M. N., & Clarke, C. J. 2001, MNRAS, 325, 781

Freeman, K. C. 1970, ApJ, 160, 811

Genel, S., et al. 2012, ApJ, 745, 11

Glover, S. C. O. & Clark, P. C. 2012, MNRAS, 421, 9

Goldreich, P., & Lynden-Bell, D. 1965, MNRAS, 130, 125

Gunawardhana, M.L.P., Hopkins, A.M., Sharp, R.G., et al. 2011, MNRAS, 415, 1647

Heckman, T. M., Armus, L., & Miley, G. K. 1990, ApJS, 74, 833

Hessman, F. V., & Ziebart, M. 2011 A&A, 532, A121

Hoekstra, H., van Albada, T. S., & Sancisi, R. 2001, MNRAS, 323, 453

Hunter, D., Elmegreen, G. G., & Baker, A. L. 1998, ApJ, 493, 595

Hunter, D.A., Elmegreen, B.G., & Ludka, B.C. 2010, AJ, 139, 447

James, P.A., Shane, N.C., Beckman, J.E., et al. 2004, A&A, 414, 23

Johansson, P.H., Naab, T., Burkert, A. 2009, ApJ, 690, 802

Jog, C. J., & Solomon, P. M. 1984, ApJ, 276, 114

Jog, C. J. 1996, MNRAS, 278, 209

Kauffmann, G., et al. 2003, MNRAS, 341, 33

Kauffmann, G., et al. 2003, MNRAS, 341, 54

Kennicutt, R.C. 1989, ApJ, 344, 685

Kennicutt, R.C. 1998, ApJ, 498, 541

Kennicutt, R.C., Jr., Bresolin, F., & Garnett, D.R. 2003, ApJ, 591, 801

Kennicutt, R.C., et al. 2007, ApJ, 671, 333

Kennicutt, R.C., Jr., Lee, J.C, Funes, S.J., et al. 2008, ApJS, 178, 247

Kobulnicky, H. A., & Kewley, L. J. 2004, ApJ, 617, 240

Krumholz, M. R., & McKee, C. F. 2005, ApJ, 630, 250

Krumholz, M. R., & Thompson, T. A. 2007, ApJ, 669, 289

Krumholz, M. R., McKee C. F., & Tumlinson, J. 2008, ApJ, 689, 865

Krumholz, M. R., McKee C. F., & Tumlinson, J. 2009, ApJ, 693, 216

Krumholz, M. R., McKee, C. F., & Tumlinson, J. 2009, ApJ, 699, 850

Krumholz, M. R., & Gnedin, N. Y. 2011, ApJ, 729, 36

Kregel, M., van der Kruit, P. C., & de Grijs, R. 2002, MNRAS, 334, 646

Lee, J.C., Gil de Paz, A., Tremonti, C., et al. 2009, ApJ, 706, 599

Leroy, A. K. et al. 2008, AJ, 136, 2782

Lin, D. N. C., & Pringle, J. E. 1987, ApJ, 320, L87

Lin, D. N. C., & Pringle, J. E. 1987, MNRAS, 225, 607

Lotz, J.M., Jonsson, P., Cox, T.J., & Primack, J. 2008, MNRAS, 391, 1137

Markwardt, C. B. 2009, Astronomical Data Analysis Software and Systems XVIII ASP Conference Series, 411, 251

Meurer, G. R., et al. 2006, ApJS, 165, 307

Meurer, G. R., et al. 2009, ApJ, 695, 765

Meurer, G. R., Zheng, Z., & de Blok, E. 2013, MNRAS, 429, 2537

Martin, C. L., & Kennicutt, R. C. 2001, ApJ, 555, 301

McKee, C.F., & Ostriker, E.C., 2007, ARA&A, 45, 565

Moustakas, J., et al. 2010, ApJS, 190, 233

O'Brien, J. C., Freeman, K. C., & van der Kruit, P. C. 2010, A&A, 515, A62

Ostriker, E. C., McKee, C. F., & Leroy, A. K. 2010, ApJ, 721, 975

Persic, M., Salucci, P. & Stel, F. 1996, MNRAS, 281, 27

Pohlen, M. & Trujillo, I. 2006, A&A, 454, 759

Quirk, W. J. 1972, ApJ, 176, L9

Rafikov, R. R. 2001, MNRAS, 323, 445

Romeo, A. B. & Wiegert, J. 2011, MNRAS, 416, 1191

Saintonge, A., et al. 2011, arXiv:1104.0019

Schmidt, M. 1959, ApJ, 129, 243

Silk, J. 1997, ApJ, 481, 703

Sofue, Y., & Rubin, V. 2001, ARA&A, 39, 137

Tamburro, D. et al. 2009, AJ, 137, 4424

Tan, J. C. 2000, ApJ, 536, 173

Tan, J. 2010, ApJ, 710, L88

Thilker D. A., Bianchi L., Boissier S., et al., 2005, ApJ, 619, L79

Thilker, D. et al. 2007, ApJS, 173, 538

Toomre, A. 1964, ApJ, 139, 1217

Tremonti, C. A., et al. 2004, ApJ, 613, 898

van den Bosch, F. C. 2001, MNRAS, 327, 1334

van der Hulst, J. M. et al. 1993, AJ, 106, 548

van der Kruit, P. C. 1988, A&A, 192, 117

Walter, F., et al. 2008, AJ, 136, 2563

Wang, B. & Silk, J. 1994, ApJ, 427, 759

White, S. D. M., & Rees, M. J. 1978, MNRAS, 183, 341

Wong, I., et al. 2013, in preparation

Wong, T., & Blitz, L. 2002, ApJ, 569, 157

Wong, T. 2009, ApJ, 705, 650

Zaritsky, D., Kennicutt, R.C., Jr., & Huchra, J P. 1994, ApJ, 420, 87

Table 1. Q_{2f} model fit results and galaxy properties

Galaxy	N_{ann}	Q_R	ϵ_{Q_R}	Q_{WS}	$\epsilon_{Q_{WS}}$	$Q_{RW,thin}$	$\epsilon_{Q_{RW,thin}}$	$Q_{RW,thick}$	$\epsilon_{Q_{RW,thick}}$	V_m [km/s]	$\log(M_S)$ [$\log M_\odot$]	$\log(M_g)$ [$\log M_\odot$]	$\frac{SFR_{cen}}{SFR_{int}}$
DDO154	4	3.50	0.10	2.80	0.10	3.26	0.16	4.48	0.19	50.00	7.10	8.70	0.20
IC2574	27	1.46	0.21	1.26	0.20	1.30	0.21	1.84	0.21	134.00	8.70	9.30	0.13
NGC7793	22	1.77	0.19	1.70	0.21	1.79	0.18	2.34	0.19	115.00	9.50	9.10	0.55
NGC2403	33	1.96	0.18	1.89	0.20	1.98	0.17	2.61	0.17	134.00	9.70	9.50	0.49
NGC0925	22	1.82	0.22	1.36	0.23	1.44	0.27	1.98	0.25	136.00	9.90	9.82	0.43
NGC3198	14	1.82	0.16	1.42	0.15	1.58	0.23	2.09	0.21	150.00	10.10	10.12	0.37
NGC4736	16	1.85	0.27	1.73	0.29	1.78	0.28	2.20	0.29	156.00	10.30	8.95	3.45
NGC6946	24	1.55	0.26	1.21	0.31	1.53	0.23	2.05	0.20	186.00	10.50	10.01	0.31
NGC3521	18	1.57	0.17	1.19	0.21	1.50	0.20	1.99	0.19	227.00	10.70	10.15	0.66
NGC5055	25	1.67	0.18	1.31	0.28	1.69	0.20	2.29	0.16	192.00	10.80	10.25	0.83
NGC2841	15	3.99	0.17	2.52	0.19	2.94	0.21	3.66	0.20	302.00	10.80	10.11	0.14
NGC7331	20	1.86	0.13	1.33	0.16	1.67	0.22	2.20	0.20	244.00	10.90	10.25	1.04
Mean		2.07	0.187	1.64	0.211	1.87	0.213	2.48	0.205	168.83	10.45	9.93	0.72

[a]Four forms of stability parameters ($\log Q$) are calculated using a fixed $\sigma_g = 11 km/s$ and then fitted using a constant. Only the intermediate disk data is used during this fitting. The fitted value and the corresponding deviation value, ϵ, for each galaxy are tabulated here. The maximum velocity V_m, total stellar mass M_S, total gas mass M_g and the ratio between the integrated central disk SFR and intermediate disk SFR $\frac{SFR_{cen}}{SFR_{int}}$ are also tabulated here (data from L08). The galaxies are listed in ascending order of total stellar mass $\log(M_s)$.

Table 2.   Model-observation deviation for gas surface densities

Galaxy	N_{ann}	$\epsilon_{\mathrm{HI_{SR}}}$	$\epsilon_{\mathrm{HI_{PR}}}$	$\epsilon_{\mathrm{HI_{KR}}}$
DDO154	4	0.02	0.13	0.02
IC2574	27	0.06	0.14	0.06
NGC7793	22	0.24	0.27	0.13
NGC2403	33	0.18	0.21	0.10
NGC0925	22	0.08	0.13	0.08
NGC3198	14	0.06	0.11	0.05
NGC4736	9	0.64	0.51	0.53
NGC6946	24	0.13	0.13	0.11
NGC3521	18	0.10	0.16	0.09
NGC5055	25	0.14	0.11	0.17
NGC2841	15	0.25	0.23	0.20
NGC7331	20	0.10	0.13	0.06
Median		0.13	0.14	0.10
Mean		0.17	0.19	0.14
		$\epsilon_{\mathrm{H2_{SR}}}$	$\epsilon_{\mathrm{H2_{PR}}}$	$\epsilon_{\mathrm{H2_{KR}}}$
NGC3198	4	0.20	0.24	0.31
NGC6946	17	0.23	0.26	0.24
NGC3521	12	0.24	0.35	0.21
NGC5055	12	0.20	0.25	0.20
NGC2841	8	0.13	0.38	0.47
NGC7331	8	0.21	0.25	0.17
Median		0.21	0.26	0.24
Mean		0.20	0.29	0.27

[a]ϵ is calculated for all three R_{mol} prescriptions. The upper half of this table is for Σ_{HI} and the lower half is for $\Sigma_{\mathrm{H_2}}$. There are less N_{ann} values in the lower half because there are fewer data points for $\Sigma_{\mathrm{H_2}}$.

Table 3.   Star Formation Law Parameters for Sample Galaxies (1)

Galaxy	N_{ann}	A_{SK} (10^{-2})	$\epsilon_{\mathrm{SFR_{SK}}}$	A_{ff} (10^{-2})	$\epsilon_{\mathrm{SFR_{ff}}}$	$A_{\mathrm{ff'}}$ (10^{-2})	$\epsilon_{\mathrm{SFR_{ff'}}}$	B_{Ω} (10^{-3})	$\epsilon_{\mathrm{SFR_{\Omega}}}$	B_{CC} (10^{-3})	$\epsilon_{\mathrm{SFR_{CC}}}$
DDO154	4.	2.51	0.155	3.28	0.156	12.49	0.159	4.01	0.062	41.62	0.128
IC2574	27.	1.66	0.274	2.14	0.274	7.49	0.272	9.49	0.273	33.78	0.343
NGC7793	22.	6.84	0.491	8.86	0.489	32.29	0.484	11.61	0.458	42.52	0.577
NGC2403	33.	6.71	0.394	8.72	0.393	32.04	0.387	10.98	0.308	57.46	0.407
NGC0925	22.	3.30	0.200	4.27	0.194	15.42	0.167	20.39	0.204	64.03	0.273
NGC3198	14.	4.96	0.200	6.41	0.192	22.42	0.145	10.51	0.152	40.55	0.246
NGC4736	9.	12.38	0.838	12.65	0.856	14.13	1.394	0.63	1.077	14.77	1.293
NGC6946	24.	16.23	0.355	19.27	0.344	43.65	0.294	23.42	0.270	82.37	0.360
NGC3521	18.	5.43	0.401	6.43	0.379	14.31	0.257	6.91	0.296	20.21	0.399
NGC5055	24.	6.83	0.520	8.58	0.505	25.73	0.418	11.27	0.418	30.35	0.468
NGC2841	15.	5.79	0.341	7.18	0.390	20.22	0.676	3.50	0.375	26.96	0.605
NGC7331	20.	4.31	0.232	5.32	0.212	14.44	0.103	5.92	0.101	14.86	0.111
All	232	9.04	0.557	11.10	0.543	28.06	0.523	12.10	0.385	39.18	0.501
Median		5.79		7.18		20.22		10.51		40.55	
Mean		6.41		7.76		21.22		9.89		39.12	

[a]The fitted SFL coefficients and model-observation deviations: SK, Schimidt-Kennicutt Law; ff, free-fall time scale with fixed scale height; ff′, free-fall time scale with variable scale height; Ω, orbital time scale; CC, GMC collisions in a shearing disk. These five SFLs only depend on the total gas surface mass density and galactic dynamic parameters. The 'All' means the fitting using all valid data points from all the sample galaxies. All the 'A' coefficients have units of $M_{\odot}kpc^{-2}yr^{-1}$ and all the 'B' coefficients are dimensionless.

Table 4.   Star Formation Law Parameters for Sample Galaxies (2)

Galaxy	A_{H_2} (10^{-2})	$\epsilon_{\mathrm{SFR}_{\mathrm{H}_2}}$	A_{KM}	$\epsilon_{\mathrm{SFR}_{\mathrm{KM}}}$	A_{KMT} (10^{-2})	$\epsilon_{\mathrm{SFR}_{\mathrm{KMT}}}$
SR relation						
DDO154	30.94	0.060	77.70	0.142	71.09	0.058
IC2574	17.70	0.255	83.59	0.204	38.85	0.251
NGC7793	13.22	0.169	40.33	0.291	29.35	0.168
NGC2403	11.33	0.108	27.99	0.165	24.20	0.125
NGC0925	9.83	0.195	61.09	0.165	20.74	0.232
NGC3198	6.90	0.181	16.08	0.193	14.19	0.229
NGC4736	11.49	0.459	1.19	1.654	11.71	0.651
NGC6946	14.80	0.159	15.28	0.197	23.46	0.146
NGC3521	5.02	0.167	4.08	0.090	7.83	0.095
NGC5055	6.72	0.269	7.81	0.135	12.51	0.196
NGC2841	3.75	0.296	4.96	0.827	7.25	0.485
NGC7331	4.37	0.056	3.84	0.261	7.65	0.138
All	9.51	0.300	8.37	0.642	15.61	0.334
Median	11.33		16.08		20.74	
Mean	11.34		28.66		22.40	
PR relation						
DDO154	3.86	0.124	11.38	0.066	8.84	0.126
IC2574	2.71	0.254	10.78	0.284	5.88	0.253
NGC7793	8.03	0.432	19.49	0.494	17.80	0.428
NGC2403	8.04	0.327	20.86	0.330	17.62	0.320
NGC0925	4.83	0.140	30.42	0.163	10.45	0.133
NGC3198	5.73	0.101	13.57	0.098	12.06	0.083
NGC4736	11.67	0.832	1.18	1.926	11.90	1.040
NGC6946	13.47	0.300	14.65	0.268	21.79	0.266
NGC3521	4.56	0.309	3.90	0.194	7.28	0.228
NGC5055	7.08	0.391	8.29	0.249	13.42	0.324
NGC2841	4.82	0.565	5.64	1.116	9.01	0.770
NGC7331	4.13	0.103	3.75	0.145	7.36	0.058
All	8.66	0.440	8.13	0.503	15.08	0.407
Median	5.73		11.38		12.06	
Mean	6.58		11.99		11.95	
KR relation						
NGC7793	76.85	0.396	223.23	0.426	167.85	0.406
NGC2403	23.20	0.422	45.28	0.504	46.87	0.445
NGC0925	15.66	0.254	98.27	0.230	32.49	0.259
NGC3198	9.09	0.898	19.59	0.915	17.84	0.931
NGC4736	12.46	0.454	1.18	1.499	12.71	0.647
NGC6946	14.11	0.268	14.88	0.255	22.54	0.238
NGC3521	5.07	0.193	4.08	0.206	7.83	0.204
NGC5055	6.44	0.190	7.54	0.232	11.90	0.209
NGC2841	3.60	0.637	4.62	0.869	6.80	0.732
NGC7331	4.22	0.295	3.67	0.409	7.24	0.360
All	9.38	0.441	8.18	0.639	15.10	0.475
Median	12.46		14.88		17.84	
Mean	17.07		42.23		33.49	

[a]The fitted SFL coefficients and model-observation deviations: H_2, linear molecular SFL; KM, turbulence-regulated SFL; KMT, two-component SFL. These SFLs depend on the molecular gas surface mass density and galactic dynamic parameters. Therefore we list fitted values for Σ_{H_2} calculated using both SR and PR relations. Results for the KR relation in DDO154 and IC2574 are omitted because eq. 16 yields non real results over much of these galaxies. All the 'A' coefficients have units of $M_\odot kpc^{-2}yr^{-1}$.